2003

Surface-enhanced vibrational spectroscopy of diphenyl sulfide and diphenyl disulfide on films and colloids, and the single-molecule detection of perylene dye on silver and gold colloids.

Ben Issa M. Ali. Tolaieb
University of Windsor

SURFACE ENHANCED VIBRATIONAL SPECTROSCOPY OF DIPHENYL SULFIDE AND DIPHENYL DISULFIDE ON FILMS AND COLLOIDS, AND THE SINGLE MOLECULE DETECTION OF PERYLENE DYE ON SILVER AND GOLD COLLOIDS

BY

Ben Issa M. Ali Tolaieb

A Thesis
Submitted to the Faculty of Graduate Studies and Research through the Department of Chemistry and Biochemistry in Partial Fulfillment of the Requirement for the Degree of Master of Science at The University of Windsor

Windsor, Ontario, Canada
2003

Your file Votre référence
ISBN: 0-612-82898-0
Our file Notre référence
ISBN: 0-612-82898-0

ABSTRACT

For more than two decades, since surface enhanced Raman scattering (SERS) phenomenon was discovered, nanoparticles of coinage metal and, in particular, colloidal metal particles and their properties have been the focus of intensive research. Various methods of preparation have been developed and the change of properties as a function of time has been studied. In this work, colloidal particles of gold and silver are used as enhancing substrates to study behavior of organic sulfides and a perylene derivative butylimido, butyleneamine perylene (*n*Bu-PTCDA-$(CH_2)_4$-NH_2) adsorbed on metal particles using surface-enhanced resonance Raman scattering (SERRS) or SERS. In addition, the SERS spectra of the adsorbed species formed by diphenyl disulfide and diphenyl sulfide (DPDS, DPS) on evaporated silver and gold island thin films were obtained. The SERS vibrational spectra of both DPDS and DPS are discussed and the vibrational assignments of the fundamental modes were aided with an *ab-intio* calculations using Density Functional Theory (DFT) at B3LYP at 6-31G (d) level of theory. The vibrational assignment, breakage or cleavage of the S-S and C-S bonds on metallic nanoparticles is discussed. In particular, the review of the observation and assignment of the Ag-S stretching vibration in the range of 150-250 cm^{-1} is provided. Three laser lines (514 nm, 633 nm and 780 nm) were used in this work to study the degree of photo dissociation induced by different energies of the incident beam. It was found that the DPDS shows cleavage of the S-S bond on both silver film, silver colloid, and evaporated gold island film. The work was extended to include the SERRS applications as sensitive techniques to be used to detect a single molecule, and track a molecular dye at nano and picomole concentrations using the colloidal silver and gold sols. The vibrational spectra of *n*Bu-PTCDA-$(CH_2)_4$-NH_2 were studied. In the infrared transmission and reflection absorption spectra were collected using Fourier transform infrared. Again, the assignment of experimental results were aided using an *ab-inito* theoretical calculations; Hartree Fock HF at 2-31G levels and DFT B3LYP at 6-31G (d) and. Fundamentals as well as overtones and combinations were observed at the concentration approaching single molecule adsorbed on colloidal gold nanoparticles casted on glass slides.

DEDICATION

I would like to dedicate this thesis to my mother, my wife, my two little daughters and my brothers and sisters.

ACKNOWLEDGMENT

I would like to thank my supervisor Professor Ricardo Aroca for his great guidance and tireless supervision, and Waha Oil Company for the great support through the years of my master study.

I would like to extend my gratitude to all past and present members of material and surface science group; Dr. C. Constantino, Dr. M. Hall, Daniel, Nik, Paul, Teo, Tibebe, Maryam, Patricia A. and Patricia Aroca, Sharon Horne as well as the secretaries in the Department of Chemistry and Biochemistry.

TABLE OF CONTENTS

LIST OF FIGURES

LIST OF TABLES

LIST OF ABBREVIATIONS

SERS Surface Enhanced Raman Scattering

SERRS Surface Enhanced Resonance Raman Scattering

SEIRA Surface-enhanced infrared absorption

SEVS Surface-enhanced vibrational spectroscopy

RRS Resonance Raman Scattering

DPDS Diphenyl disulfide

DPS Diphenyl sulfide

DFT Density Functional Theory

HF Hartree Fock level of calculation

EM Electromagnetic

CT Charge-transfer

HOMO Highest occupied molecular orbital

LUMO Lowest unoccupied molecular orbital

UV-visible Ultraviolet-visible

SMD Single Molecule Detection

SMS Single Molecule Spectroscopy

α The induced molecular polarizability

E Amplitude of the electric field

μ Dipole moment

$h\nu$ The energy of the photon

DBDS Dibenzyl Disulfide

LB Langmuir-Blodgett

CCD Charge coupling device

N.A Numerical aperture

FT-IR Fourier transforms infrared

MCT Mercury cadmium telluride

TS Transmission spectroscopy

ERS External reflection spectroscopy

IRS Internal reflection spectroscopy

RAS Reflection Absorption Spectroscopy

6-31G(d) Basis set

TFA Trifluoroacetic acid

PTCD Perylene tetracarboxylic acid

AFM Atomic Force Microscopy

a.u Arbitrary Unit

1. INTRODUCTION

1.1 Metal colloids (hydrosols)

Metal colloids (sol) have a great impact and play a significant role in Surface-Enhanced Raman Scattering (SERS) as a common substrate in the study of adsorbates on nanostructures. The structure, conformation, orientation and binding mechanism of molecules adsorbed on colloidal metal nanoparticle such as silver, gold and copper can also be studied. These optically active metal substrates have been employed for SERS investigation since the early days of SERS discovery.[1,2] In the past two decades, SERS applications, preparation and characterization of physical and chemical properties of metal colloids have increased. SERS has been discussed extensively in the literature. We can select two reviews[3,4] to illustrate the ongoing discussion on various aspects of SERS. It is generally accepted that two separate enhancement mechanisms, namely, electromagnetic (EM) and charge-transfer (CT) mechanisms could operate and contribute to the observed SERS. In the EM mechanism, the induced surface plasmon excitations, for which the surface roughness is important, at or near the resonance gives rise to an electric local field enhancement. Since the EM model is independent of the adsorbed molecule in accounting for the response of the metal surface, it cannot distinguish the difference between the adsorbed molecules. Other studies show the properties of SERS when the chemisorption or short- range chemical bond exists.[5,6] The CT theory uses the specifics of the electron transfer between the Fermi level and the HOMO-LUMO levels of the free molecule. The basic idea is that the resonance scattering is caused by the CT transition between the active surface and admolecule.

Silver and gold colloids have been used in this work. We have used different methods of preparation and studied the effect of aging on the optical properties. In addition to SERS, surface-enhanced resonance Raman scattering (SERRS) has been obtained for a number of adsorbate molecules. The preferred approach to study molecular orientation and kinetics is using silver and gold nanoparticles.[7,8] Ramos[9] has examined the effectiveness of adding certain ions and the impact of this addition on the surface morphology of the particles. We have not used additional ions in our work. However, extraneous bands in the SERS spectra could be seen as a result of the non-reacted ions of the salts used in the reduction process during preparation of colloidal solutions, e.g $NaBH_4$, $HAuCl_4.4H_2O$[10]. Recently, several research groups have studied the intrinsic surface enhanced Raman properties of single silver and gold colloidal nanoparticles.[10-12] The results indicate that a very small fraction of colloidal nanoparticles are highly efficient for optical enhancement, yielding an enhancement factor on the order of 10^{14} to 10^{15}. Nie *et al*[13] reported a technique to obtain nanoparticles using a fractionation method for what different size of colloidal nanoparticles in the range of 30-100 nm can be prepared. Moskovits[14] and his co-workers reported that SERS could also be obtained for phthalazine adsorbed on the colloidal silver aggregates as a function of cluster size deposited on the glass slide. The micro-size of the colloidal cluster form fractals whose optical properties have been the subject of considerable literature.[15,16] Creighton[17] was the first to report the copper colloids and their properties to be used as an active substrate. Both the absorption spectra and the dynamic light scattering suggest that the aggregated copper sols are quite poly-disperse in nature. Furthermore, the individual colloids are rather widely separated in the solution.

1.1.1 Colloidal stability

Colloid stability refers to the ability of dispersion to resist coagulation (aggregation). The stability of dispersion may be either kinetic or thermodynamic and has been traditionally the primary concepts of colloid science. Kinetic stability is a consequence of a force barrier against collisions between the particles and possible coagulation subsequently. The aggregation is preferred in some cases because of the resulting reduction in thermodynamic free energy, but the interaction energy barrier in the interparticle energy is larger than the thermal energy. The Van der Waals force between the particles cannot be neglected and in dispersion it is usually attractive and strong at short interparticle separation. Therefore, if there are no repulsive interactions between particles, the dispersion will be unstable and aggregates may be formed (coagulate). The protection against Van der Waals attraction is usually provided by different ways: first, surfaces of colloidal particles typically acquire charges for a number of reasons. The electrostatic force, that results when the electrical double layers of two particles overlap, if repulsive, serves to counteract the attraction due to Van der Waals forces. The stability in this case is known as electrostatic stability, and our task is to understand how it depends on the relevant parameters. Second, electrostatic repulsion is not always a convenient option. In such cases, a suitable polymer that adsorbs on the particle surfaces may be added to the dispersion. The resulting polymer layer masks the attraction and may also provide a repulsive force, partly due to pure steric effect, when the polymer layers on two interaction particles attempt to overlap with each other. This is known as polymer induced stability. Polymer induced stability is often referred to as steric stability for the above reasons.

In case of most sols, polyvinyl pyrolidone[18] is usually added as stabilizer in a concentration of 0.01%. Figure 1 shows the stability of silver colloids prepared using borohydride as a reducing agent. The shift of the plasmon absorption after ten weeks from 391 nm to 396 nm and the reduction of the absorbance values might be due to the liquid evaporation and the increase of silver particle aggregation. SERS of phenyl sulfide on silver citrate colloids showed no difference after a long storage except the increase of the SERS signal of DPDS; this means the colloidal solution becomes a more transparent liquid, due to the aggregation of silver nanoparticles. A gold colloid prepared using borohydride, as a reducing agent did not last more than two weeks prior to collapse, the resulted fractal shown in Figure 2, stabilizer was not used in any colloids prepared.

1.1.2 Optical properties of the composites

The giant enhancement of optical response in metal nanocomposites and thin metallic films containing nano-scale surface features has been intensively studied in the last twenty years.[3,19,20] This enhancement is associated with the excitation of surface plasmon, collective electromagnetic modes whose characteristics depend strongly on the geometric structure of the metallic component of the medium. The silver and gold colloidal nanoparticles and their optical properties fluctuation as a function of time were observed and recorded. The colloidal silver particles have an average of 10 nm in diameter in a well distribution form and fractal aggregation can also be achieved by using a well-established method of preparation. Normally, the fractal fabrication process consists of distinct phases: the growth of the colloidal particles and then the formation of the fractals. In this particular study, the two ways of growing colloidal gold and silver

particles were Lee-Meisel's[21] and Creighton's[22] methods. The difference between the two methods is that the first uses a trisodium citrate as a reducing agent and the latter uses the sodium borohydride as a reducing agent. Although both preparation methods result in the formation of colloidal solutions of silver particles with the diameters of the order of 10 nm, it was observed that Lee-Meisel's method results in colloidal solution possessing a higher silver concentration.[23] In the latter, it was also reported that the fractal aggregation was promoted with the addition of fumaric acid as an external aggregating agent. It was not the case in our findings when prepared gold colloids spread on a glass slide, it was left to dry in air and used to study the (DPDS) and (DPS). Fractals can clearly be seen on gold colloids even when none of the aggregating agents were added (Figure 2). Furthermore, this colloid was only stable for two weeks. To extend that, silver colloids prepared using the two mentioned methods were left for months (aged colloids) to be able to track the changes of their extinction coefficient and optical properties using UV-vis. Figure 1 shows that the citrate colloid tends to aggregate more than borohydride colloids as shown by the red shift in the maximum absorption. The shoulder at the region just below 400 nm is additional evidence of aggregation; it might be associated with the presence of larger spheres, spheroids, or aggregates particularly chainlike aggregates.[24] The shoulder was noticed in the freshly prepared citrate colloids and after two months and a half of storage, while for borohydride colloids the shoulder is barely seen. Besides, the borohydride has a better particle distribution as indicated by the sharper absorption band. The small shift to a higher wavelength of the maximum absorption with the time suggests a slight aggregation for the borohydride colloids. Both colloids were stable for months. Regarding the SERS activity of Lee's colloid, it was found that it is not

necessary to ripen since the colloids are stable and reproducible.[25] In our case, the SERS signals of DPDS spectra collected by using aged citrate colloid were more intense when the 514.5 nm laser line was used. That could be due to the aggregation factor and the availability of suitable hot spots within the aggregation microcavities in the colloidal form.

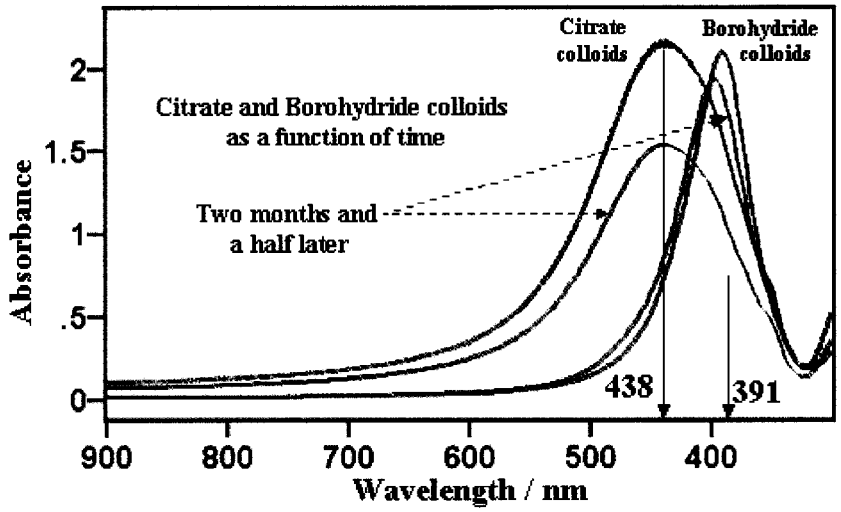

Figure 1: Borohydride and citrate colloids stability as a function of time.

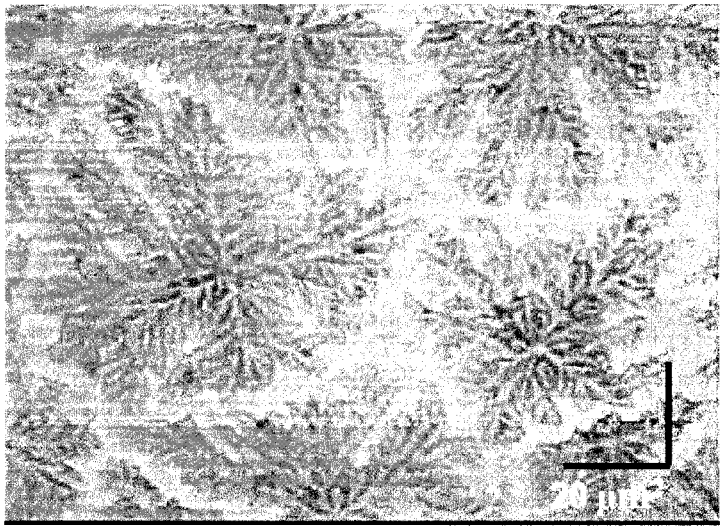

Figure 2: Gold fractal from cast gold colloids.

1.2 Raman scattering theory

The understanding of the Raman scattering is immensely important to interpret what really happens when the incident beams hit the molecule under study. The Raman scattering process is an inelastic scattering of a photon by the targeted molecule (e.g Single Molecule Detection SMD) or molecules (e.g average SERS). In addition, the incoming photons may lose their energy to the sample as a result of collision, which causes the molecule to either vibrate or rotate in the excited state. The scattered light contains frequency components that are shifted from the incident frequency by different amounts. The magnitude of these shifts is independent of the wavelength of excitation. The frequency composition of the scattered radiation is the Raman spectrum of the molecule. Light scattering actually arises from the dipole moments induced in atoms or molecules by the incident field. Through the polarization of the electrons, the static polarizability leads to Rayleigh scattering, while the modulation of the polarizability by electronic, vibrational or rotational motion leads to Raman scattering.[26] The electric field (E) induces a dipole moment (μ), which is given by equation (1) where α is the induced molecular polarizability:

$$\mu = \alpha \mathrm{E} \qquad (1)$$

The simple feature of Raman scattering is that a laser illuminates the sample with frequency v_0 and amplitude of the electric field given by equation (2):

$$\mathrm{E} = \mathrm{E}_0 cos(2\pi v_0 t) \qquad (2)$$

Suppose the polarization of the molecule is modulated at the vibrational frequency v_1, then

$$\alpha = \alpha_0 + \alpha_0 cos(2\pi v_1 t) \qquad (3)$$

where α_0 is the polarizability at the equilibrium nuclear geometry.

It is also important to note that the energy change of the molecule when interacting with a photon is equal to the energy of the photon, hv. Thus depending on the frequency of the radiation from the source, the energy of the molecule can assume any of an infinite number of virtual states between the ground electronic and first excited electronic state. In Raman spectroscopy, an intense, monochromatic incident beam passes through the sample and the radiation-scattered is detected and analyzed. The spectrum consists of a strong Rayleigh component at the incident frequency, which arises from elastic collision between the photons and the sample, and a series of lines to high and low frequency of that component. The lines at lower frequencies are the Stokes lines. They arise from the collision in which the photons lose energy to the molecules. The lines at higher frequencies are the anti-Stokes lines, and are due to collisions in which photons gain energy from the molecule. The Stokes line is stronger in intensity than the anti-Stokes at room temperature because the latter requires the presence of a pre-existing population of excited molecules. However, as temperature increases, a large fraction of the molecules will be in the first vibrational excited state and the ratio of anti-Stokes to Stokes intensity increases.[27]

1.3 Surface-enhanced Raman scattering (SERS)

SERS is the process in which the Raman scattering cross-section of molecules adsorbed onto the surfaces of metals such as silver, copper and gold is increased up to 14 orders of magnitude. More than a quarter of a century ago, Fleischmann and co-workers

observed a very strong enhancement of the pyridine Raman signals used as analyte on a roughened electrode of silver deposited electrochemically.[28] The theoretical approach as well as the molecular responses to such a giant electrical field has been subject of different studies.[29] The mechanism of the SERS was investigated by *ab initio* molecular orbital theory.[30] Corni and Tomasi[31] explored one of the most recent theoretical evaluations of the Raman intensity for a molecule adsorbed on a metal particle aggregate in the presence of solvent. The molecule was also treated at *ab initio* level for the evaluation of the ground state electronic density and nuclear geometry. In the early days, the huge Raman signal scattered from the rough surface was thought to be as a result only of the roughness of the substrates.[2] A purely physical mechanism was proposed in which the molecules were presumed to respond to a gigantic electromagnetic field generated locally by the collective oscillations of the free electrons in small metal structures. In addition, so-called chemical mechanism envisioned charge transfer between metal and adsorbate or else formation of molecule-atom complex. Recent studies[32] have proved that the contribution of chemicals (chemical effect) used to coat the surface is two to three orders of magnitude.

1.4 Phenyl and diphenyl disulfides

Sulfur containing organic compounds such as thiols and disulfide are well known as effective surface-active agents. They are widely used to prevent the corrosion of metals and to treat the surfaces of materials, however their chemical processes at the surfaces are not well understood.[33,34] Recently, there have been a few studies about the behavior of this class of molecules on metal surfaces.[35-39] The structural formula of the

DPS and DPDS molecules are shown in Figure 3. Several groups have investigated the vibrational spectra and the surface-enhanced vibrational spectra of sulfide derivatives. The most extensive study of the cleavage of the C-S and S-S bonds for a number of alkyl and aryl sulfide derivatives on silver has been carried out by Kim's group.[40] The cleavage of these chemical bonds under mild conditions may have several technological applications. Sandroff and Herschbach[36] first reported the cleavage of the S-S bond due to chemisorptions of DPDS onto rough silver surfaces in SERS. Notably, the Ag-S stretching vibration was assigned for DPDS and dibenzyl disulfide (DBDS) by comparing their SERS spectra with the observed SERS spectra of thiophenol (benzenethiol or phenyl mercaptan) and benzyl thiol. The Ag-S in aromatic thiols is formed by chemisorption on silver following dissociation of the S-H bond. A weak band at 246 cm^{-1} in SERS spectrum of thiophenol on silver and also a weak band at 302 cm^{-1} in SERS of benzyl thiol have been assigned to Ag-S bond. Since sulfur is a soft atom and the Ag-S is likely to be perpendicular to the surface, the relatively low Raman intensity is in doubt. A higher vibrational wavenumber for the heavier molecular complex (302 cm^{-1}) is also unusual. Sandroff and Herschbach assumed a thiophenolate lying flat on the surface, which would explain the low relative intensity in the SERS spectrum.[41] However, Takahashi *et al.*[42] reported a head-on adsorption of the thiophenolate. Similar head-on results were recently reported in surface-enhanced infrared absorption (SEIRA) of P-nitrothiophenol and its disulfide by Merklin *et al.*.[38] The SEIRA studies further suggest that there are indeed two types of chemisorbed species, including the adsorption of the undissociated bis(p-nitrophenyl)disulfide with both sulfur attached to the silver surface. In the infrared studies, the Ag-S is below the wavenumber range reported (mid-

IR) requiring deeper investigation in far-IR. In a separate SERS study of the thiophenol on silver colloids, Kim *et al.*[43] reported a very weak shoulder at 237 cm^{-1} as the Ag-S bond stretching, and conjectured that the complex was adsorbed face-on the silver surface. Kim's group clearly established that dialkyl sulfides do not undergo C-S cleavage on silver, while the opposite was observed for the disulfide derivatives with facile cleavage of the S-S bond.[18]

The relative intensities of the observed bands in the SERS spectrum may be quite different from the vibrational spectrum of the material used to coat the enhancing surface. Light polarization at the metal surface, molecular orientation or photodissociation, could be responsible for that, leading to a low relative intensity of the metal-S bond.

1.5 Single molecule spectroscopy (SMS)

Following the discovery of SERS about twenty-five years ago, there was unpredicted focusing of research on this part of science. A giant average enhancement $\sim 10^6$ in the Raman signals associated with vibrational excitation of the pyridine molecule adsorbed on silver electrodes in an electrochemical cell were achieved.[44,45] Since the study of the surface adsorbate on the active surface by surface-enhanced vibrational spectroscopy (SEVS), the latter became a useful tool as an analytical technique to obtain and understand the behavior of a molecule or molecules and their interaction with different surfaces, and surrounding environment. Detecting a single molecule in a solution with high sensitivities and molecular specificity is of great scientific and practical interest in many fields such as chemistry, biology, medicine and environmental science.[46] The sensitivity of Raman scattering techniques comes from the strongly

increased Raman signals per molecule, which has been attached to nano-scale metal particles. These large effective Raman cross sections on the order of (10^{-17}-10^{-16} cm^2/molecule) included the Raman technique into the hall of those used for observing single molecules.[47] It was also found that the enhancement factor as large as 15 orders of magnitude could provide Raman cross section as high as (10^{-16} cm^2/molecule).[19,48-52] Theoretically, a very small fraction of nanospherical particles, simulating the presence of aggregates, may count for the very strong red-shifted UV-vis absorption peak, which in turn may be accompanied by a hardly perceptible shoulder in the extinction spectrum of the colloidal sols at the corresponding wavelength.[29] Moreover, practically, colloidal aggregating agents are commonly used to improve the analyte detection level.[53,54] The aggregates or clusters formed are shown to provide a very high enhancement factor.[55-57] The size of these metal clusters, ranging from 100-1000 nm in size, provides a suitable enhancing substrate to detect even a single molecule in liquid form. The molecule has a certain role to play in forming the aggregated clusters at which the optical field is intensively enhanced at those hot spots[10,11,52] and that depends on the size and shape of these clusters. In addition, the collective oscillating charges on the surface of these metal particles could enhance the optical field at the surface and give rise to the surface plasmon.

A spatially resolved SERRS of organic molecules at the single molecule level has recently drawn a significant interest. After the first recognition of the resonance effect in early fifties by Shorygin[58], it was three decades until Van Duyne[59] first elucidate the concept of spatially resolved SERRS. The spatially resolved SERRS is usually achieved by incubating a colloidal solution of silver or gold particles with a very low concentration

of dye molecules, less than one molecule per probed volume on average. The SERRS effect was found to increase the Raman cross section to the point where it renders the intensity of the SERRS signal comparable to that in single molecule fluorescence.[48,49, 51,60] Very recent, Meixner[61] and co-workers has studied the SERRS of single molecule of rhodamine 6G (R6G) as a function of time, which reveals an inhomogeneous behavior of intensity fluctuation (blinking). Within our research group, intensive studies were performed using different substrate preparation techniques; from colloidal solutions[62,63] where analyte of attomole concentration was detected and the use of Langmuir-Blodgett (LB) films as an alternative surface technique for detecting a single molecule.[64,65] Although the resonant excitation is attractive, it was found that it promotes the photo bleaching, especially under what is called a double resonant condition.[66] Moreover, Scholz[67] reported that for organic semiconductors such as perylene derivatives, the resonant Raman spectra are mainly determined by the vibrational excitation of an isolated molecule. In general, the electromagnetic enhancement and chemical enhancement mechanisms are well known to be the major contributors of the whole effect. The first involves the surface roughness feature and the latter involves in the charge transfer between the metal and the adsorbate when a surface complex is formed[68], which causes the electronic state of such adsorbate to change.[69] The co-existence of $-NH_2$ at one of the terminals makes it possible for the molecule to be attached in a chemisorbed fashion to the active surface. SERS and Resonance Raman Scattering (RRS) combinations appear when an adsorbate has an absorption band at the same region of the metal surface plasmon and the excitation line, which could lead to an enhancement as large as 10^{10}-10^{15}.

1.6 The thesis structure

In general, this project has concluded different aspects about the application of SERS and SERRS in characterizing materials such as sulfides and perylene derivative on metal surfaces, which have different industrial applications. Silver and gold nanoparticles were used as surface substrates, whose optical properties were also studied and investigated. Moreover, the vibrational spectra of DPS and DPDS whose molecular structure are shown in Figure 3 have been investigated as well as their peculiar behaviors when adsorbed on metal surfaces. Two different rough metal surfaces (colloids of silver and gold, evaporated films of silver and gold islands) and three different laser lines (514.5, 633 and 780 nm) have been used to obtain the SERS spectra of DPS and DPDS. DPDS was casted on evaporated silver island films from its solution in methanol or added to colloidal silver and also evaporated on evaporated gold island films to obtain SERS measurements. The work using the metal nanoparticles has been extended to approach single molecule detection using SERRS technique and having *n*Bu-PTCDA-$(CH_2)_4$-NH_2 (Figure 3) as a target molecule. The SERRS spectra from nanomole and picomole concentrations of *n*Bu-PTCDA-$(CH_2)_4$-NH_2 in the colloidal silver solution and cast gold colloidal solution on glass slide were obtained.

This thesis is structured as following: in the first chapter, the results on silver and gold metal colloids, which include colloid preparations, optical properties and topographic features of dried colloids, are presented. All of the experimental work and the instrumentation used throughout this work are described in chapter two. The third chapter contains a detailed study of DPS and DPDS using Raman and FT-IR spectroscopic techniques. In chapter four, the approach to single molecule detection

(SMD) on the colloidal metal surfaces using SERRS as a sensitive detecting technique is discussed. Finally, the conclusions are presented in chapter five.

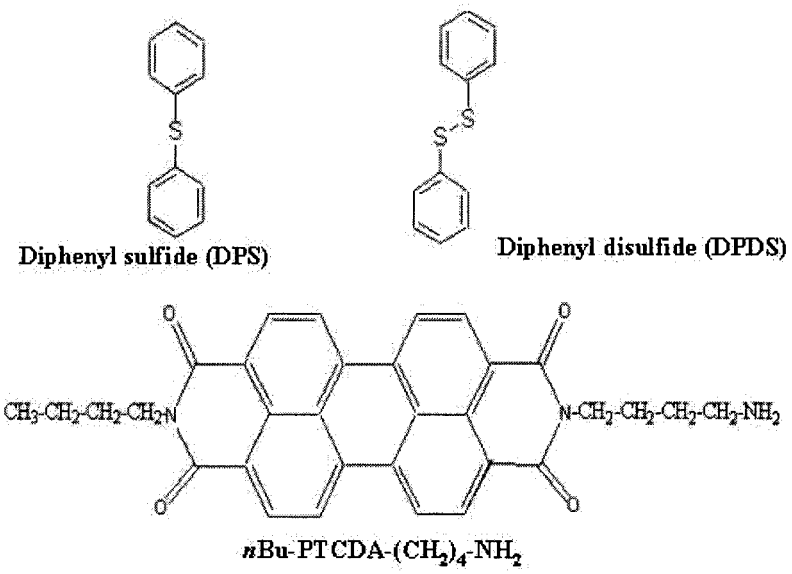

Figure 3: The structural formula for the studied molecules.

2. EXPERIMENTAL AND TECHNIQUES

2.1 Colloid preparation and properties

Since the early days of SERS and SERRS, roughened film was the only substrate preferred and finding other methods to prepare an alternative active substrate was quite a challenging subject. Although surface-enhancement can be observed on solid metal surfaces with appropriate roughness, the use of silver and gold sols as SERS-active substrate has some advantages. First it is easy to prepare, second, continuous renewal of the surface by the exchange of the colloidal suspension in the path of the laser beam, and third, it is possible to control size and shape of produced nanoparticles. In addition, taking the UV-vis spectrum can check the stability of the colloidal particles through a period of time. There are different ways of preparing the colloids of the silver, gold and copper. They all share the idea of reduction of metal ions. The major two applicable and widely used procedures are those whose reducing agents are trisodium citrate and sodium borohydride. In this work, the preparation of silver and gold sols was the backbone of major investigations, triply and highly purified distilled water was used for making the primary solutions. The silver and gold colloid preparation steps will be taken into sequence manner as following:

2.1.1 Silver colloid preparations

Borohydride colloids: this method is widely used and described elsewhere in the literature[22,70]. Simply, 10 mL of aqueous silver nitrate (10^{-3} M) is added drop-wise to 30 mL of ice-cold aqueous solution of sodium borohydride (2.0×10^{-3} M) while it is

vigorously stirred, an excess drop of silver nitrate could turn the whole solution to black. The yellowish color with a UV-vis absorption band at 391 nm shows that the silver colloids are usually stable for several months. Figure 1 shows the absorption spectra of the same silver colloidal solution prepared using borohydride with time difference.

Citrate colloids: it is a different method of preparing silver sol[21] and is expected to be suitable for single molecule detection. It is simply prepared by adding 1 mL of 1%(w/v) trisodium citrate aqueous solution to 50 mL of boiling 10^{-3} M silver nitrate aqueous solution, which is kept boiling for further 1 hour. The resulting colloid shows a turbid gray color with UV-vis absorption maximum at 408 nm (Figure 4). Although its microscopic properties can change with the time, it was stable for several months. Figure 4 also shows that different particle distributions were obtained using same method of preparation in two different occasions. The AFM image of citrate silver cast colloid without organic (a) and with organic additives (b) is shown in Figure 5. The aggregated clusters were increased to approximately the double in size when the DPDS is added. Apparently, DPDS plays a certain role in the process of aggregation.

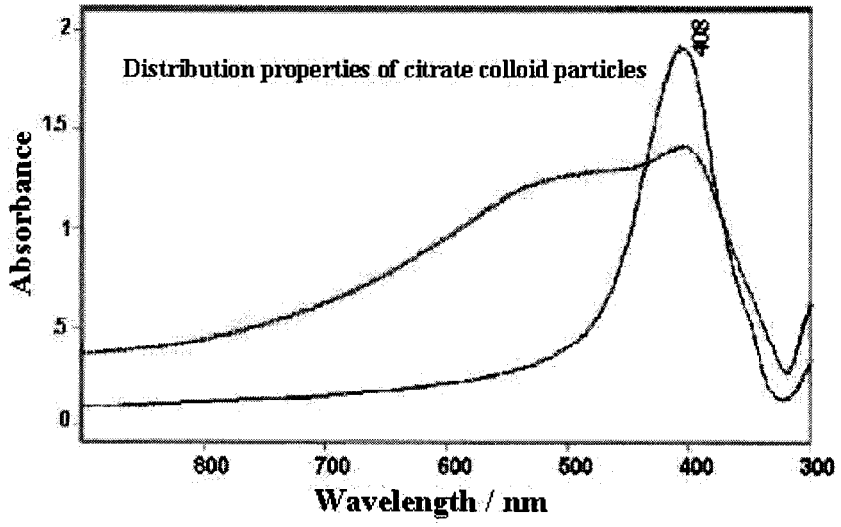

Figure 4: The silver citrate colloids with different particle distributions.

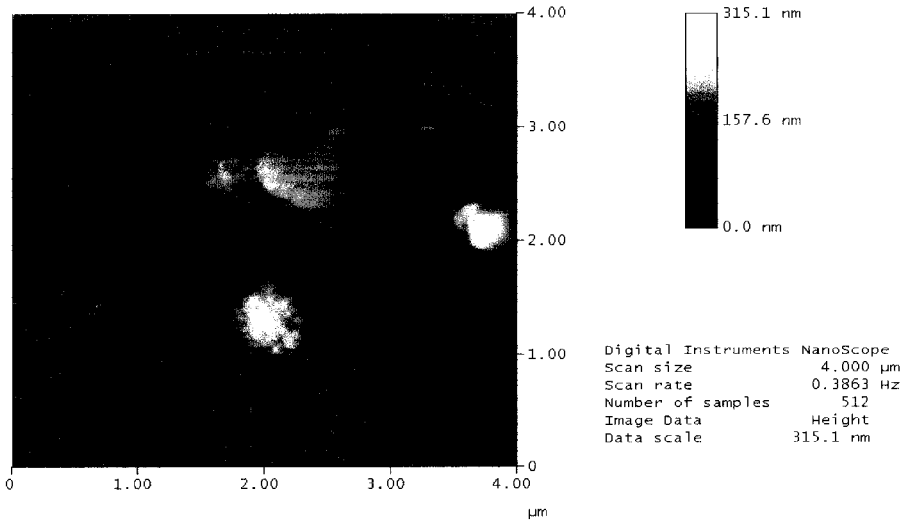

(a) AFM image of organic free silver citrate colloids

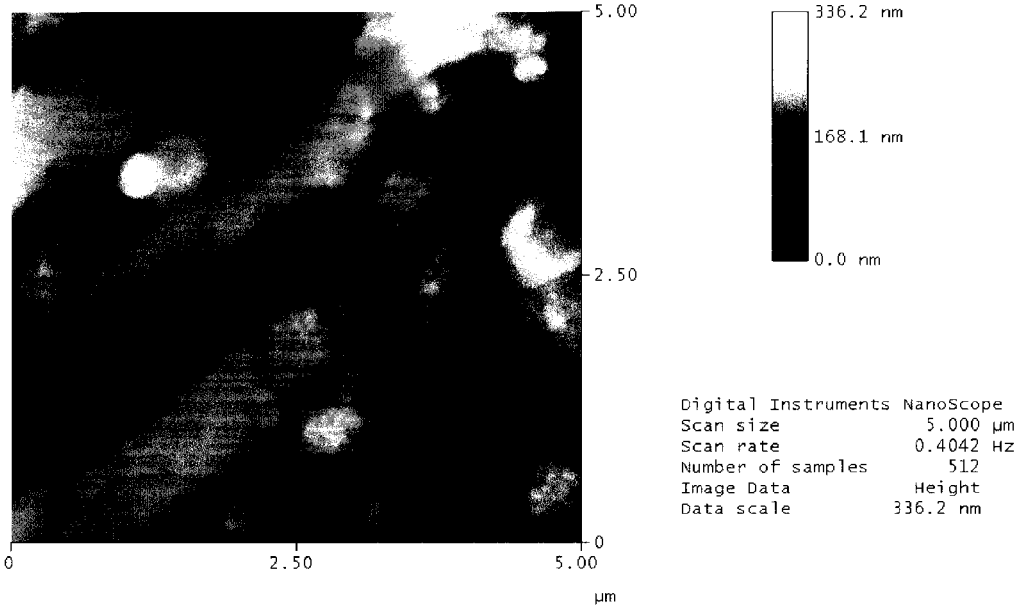

(b) AFM image of DPDS mixed with silver citrate colloid.

Figure 5: The AFM images of cast silver citrate colloids (a) without and (b) with organic additives.

2.1.2 Gold colloid preparations

Citrate colloids: preparations of silver and gold colloids using trisodium citrate as a reducing agent are alike with little changes. Ramos[71] gives the outlines for the preparations of gold sols: 0.1 mL of $HAuCl_4$ solution (4%, w/v) is added to 40 mL triply distilled water and 1 mL of trisodium citrate solution (1%, w/v) is then added drop by drop while stirring. The resulted mixture is boiled for five minutes and during this time the solution turns slowly to violet color. The first borohydride gold colloid gave a UV-vis absorption maximum at about 520 nm. It was stable for two weeks only and gave a fractal structure shown as an inset in the Figure 6. Kim[72] had used $KAuCl_4 \cdot 3H_2O$ as a starting material and citrate as a reducing agent and the colloidal UV-vis absorption band has a maximum at 532 nm. Figure 6 shows the maximum absorption of the citrate gold colloids at 527 nm. It was the second gold colloids prepared and gave an absorption maximum at 527 nm. Both were prepared using different reducing agents, the second was stable for months.

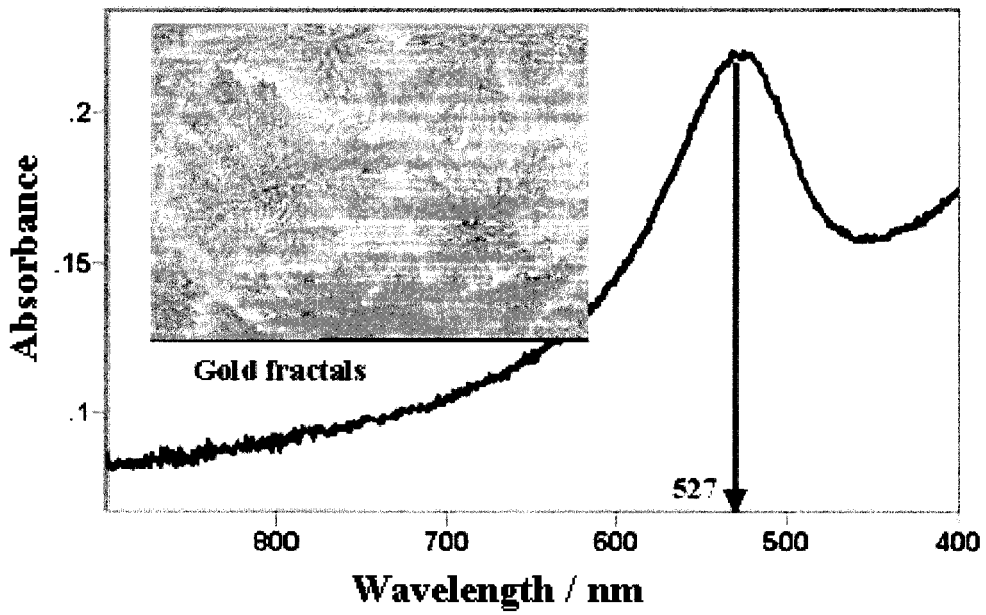

Figure 6: UV-vis maximum absorption of citrate gold colloids at 527 nm.

Copper colloids can be prepared and used for SERS studies by the following procedure.[73] The other technique of colloidal preparation using Laser-Ablation, which has also been applied by many research groups[73,74], in particular that of Prochzka[75], and Cotton.[76] This technique is a novel approach to obtain chemically pure and stable metal colloids in aqueous media, without difficulties imposed by residual ions as observed in chemically prepared metal colloidal solutions. Laser-ablated silver colloids are the most common, other metals[77] such as copper[78]and alkali metal colloids such as calcium[79] have also been reported.

2.2 Colloid statistics

The colloid statistics have been assembled based on the Sci-Finder search and is representative of the last decade of SERS activity using colloidal systems. The statistics in Figure 7 provides some information about the use of the most important nanoparticles, which are the gold and silver colloidal metals. It is observed that, in the mid nineties, the use of gold colloids was intensified. This increase in the use of gold colloids in SERS might be due to the stability of gold colloids for months and less contamination unlike in the silver colloids case. In many cases, the gold is less reactive with the additives than silver.

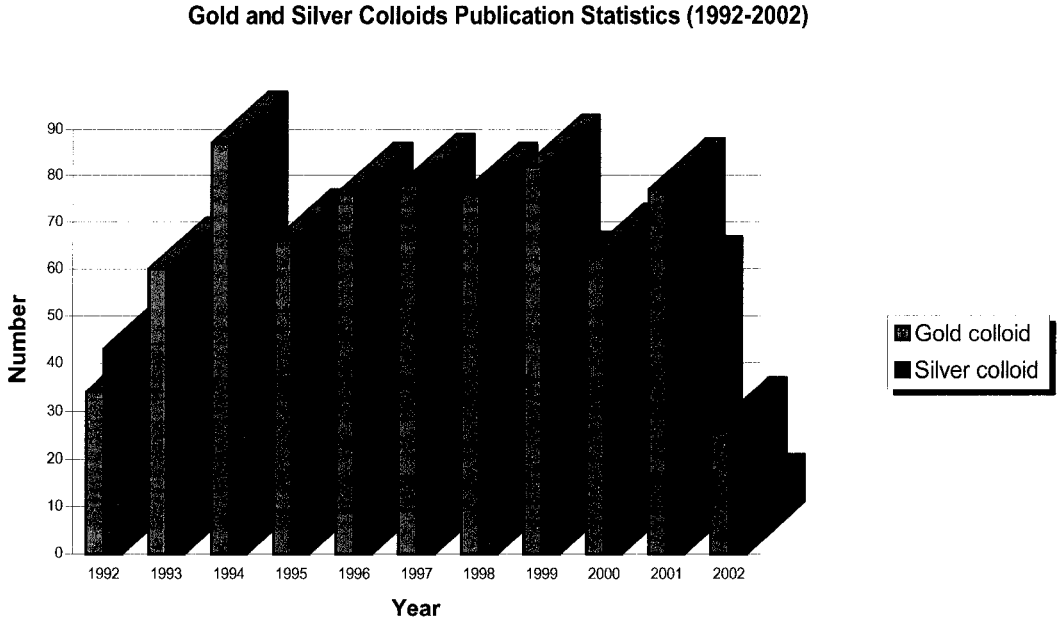

Figure 7: SERS activity on both silver and gold colloids within last decade.

2.3 Raman instrument

In the recent two decades, Raman spectroscopy has become one of the most powerful techniques for tracking and detecting trace amount of dissolved organics, especially after the discovery of the SERS phenomena. The Raman efficiency comes from the use of adequate filtering and detecting components.

The SERS and SERRS were collected by Renishaw RM2000 (Micro-Raman System) equipped with the computer controlled 3-axis encoded (XYZ) motorized stage. The system is also equipped with a Leica microscope (DMLM series) and with a Peltier cooled CCD array (-70°C) (Figure 8).[80] The spectrograph contains a 1200 grooves/mm grating with additional angle-tuned bandpass filter optics. Three laser lines (514.5 nm laser line of a Spectra-Physics argon ion laser Lexel 95, 633 nm He-Neon laser line and 780 diode laser line) were used as the power source for excitation. The power at the

sample ranged between 0.01-1 mW. When using colloids as a substrate for SERS or SERRS, 100% power (1mW) was used throughout the measurement with all laser lines using an oil immersion microscopic objective (N.A 0.80), which focus the laser beam in a scattering volume less than a nanoliter. For evaporated organic films on the silver or gold island films a 50x microscopic objective is used, which focus the beam on the surface in scattering area of about 1 μm^2. The surface power as low as 1% (0.01-0.02 mW) was used to minimize photo dissociation, which might be induced by excitation lines. It could result in unexpected bands in the spectrum if high power is applied. The numbers of scans were ranged from 5-100 scan throughout this work.

The confocal condition advantages of this instrument could increase the spatial resolution of the system. Although most of the spectra were taken at the room temperature, the instrument is also equipped with a thermostatted cell device. Data acquisition and analysis were carried out using the WIRE software for windows and Galactic Industries GRAMS^{TM} C software.

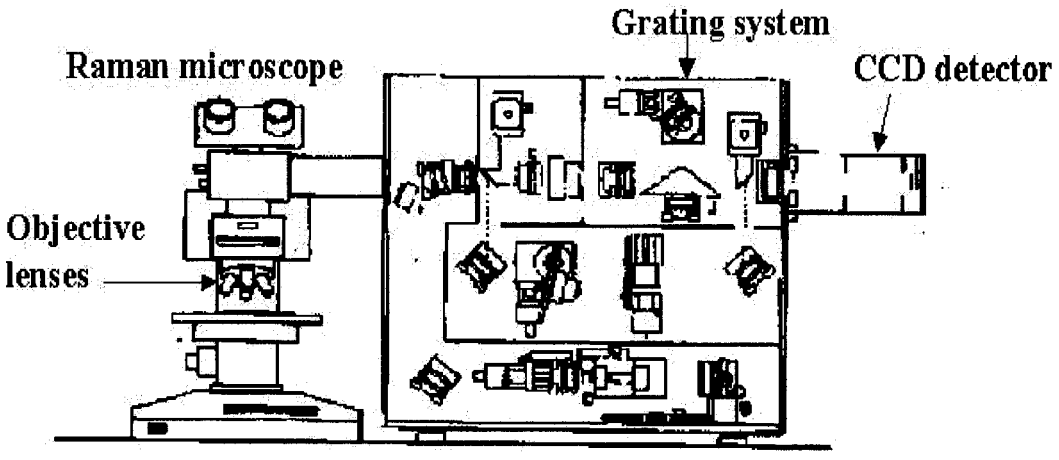

Figure 8: Renishaw Raman Microscope 2000 instrument.

2.4 Infrared absorption

In infrared spectroscopy, a light with broad band is passed through a sample and the intensity changes of the transmitted light are measured. At the vibrational energy of the sample, more light is absorbed and less transmitted. In this work, there were two FT-IR instrument used to obtain either the transmission spectra or reflection spectra of the subjected molecules, Bomem DA3 FT-IR, which has a vacuum advantage, and Bruker EQUINOX 55 Microscopic FT-IR. A brief description of both techniques is given below and sketches are shown.

2.4.1 Fourier transform infrared instruments (FT-IR)

The Bomem DA3 Fourier transform infrared spectrometer was one of the equipments used for collecting transmission and reflection FT-IR spectra. The spectrophotometer is an example of a multiplex instrument, in particular the Michelson interferometer. In this device, a beam of radiation from the source impinges on a KBr beam splitter, which transmits approximately half of the radiation and reflects the other half. The resulted twin beams are reflected from mirrors, one is fixed and the other is movable. The twin beams then meet again at the beam splitter, half of each beam is directed to the sample and MCT liquid nitrogen cooled detector and the other two halves directed back towards the source. The only two halves that pass through the sample are responsible for giving the analytical data. The optical configuration of the Bomem DA3 FT-IR spectrometer[81] is shown in Figure 9.

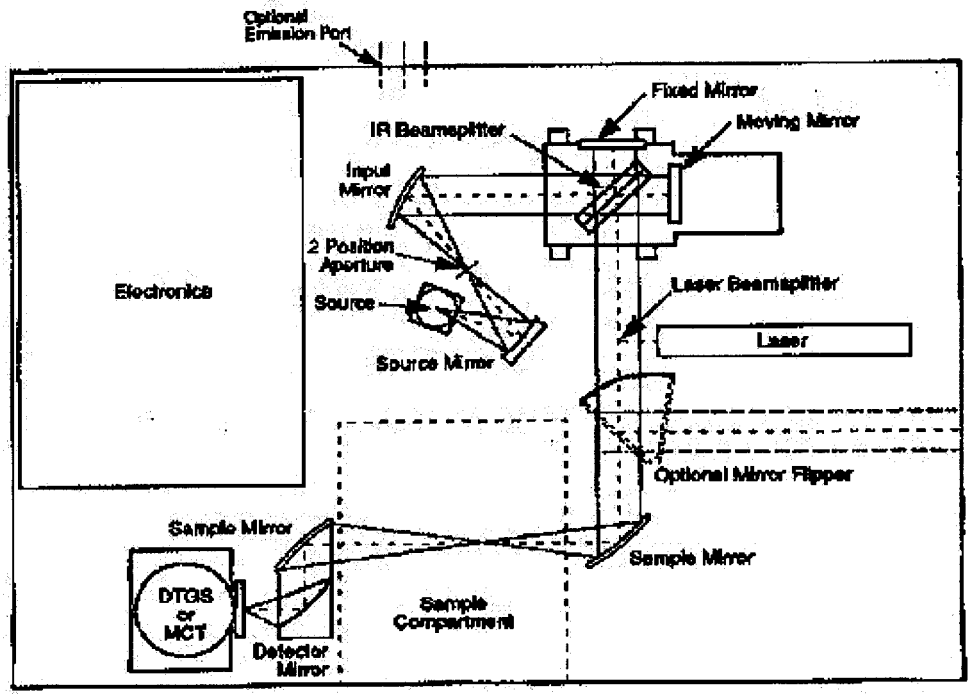

Figure 9: The optical configuration of Bomem DA3 FT-IR instrument.

The other FT-IR instrument used for collecting the infrared spectra was a Bruker EQUINOX 55. This instrument is equipped with an Auto Segall system in which the angle of reflection can be switched in a range of 0-90° without moving the sample. It is a fast and reliable for giving an accurate angle of reflection. Switching the beam between back and front paths enables the microscopic reflection or transmission. One of the unique advantages is that the possibility to have a microscopic image of the sample under study so that the focus to the point of interest is also possible. Figure 10 shows the standard optical path for the EQUINOX 55. Additional mirrors can be added to enable external routing of the IR beam (optional). In Figure 10, the IR source is located at the back of the spectrometer. A parabolic mirror collects the IR light emitted by the source, to create a parallel beam. The following flat mirror directs it to the interferometer. An additional parabolic mirror diverts the beam leaving the interferometer into the sample

compartment to focus the beam on the sample positioned in the center. After exciting the sample compartment the beam is then focused on the detector.

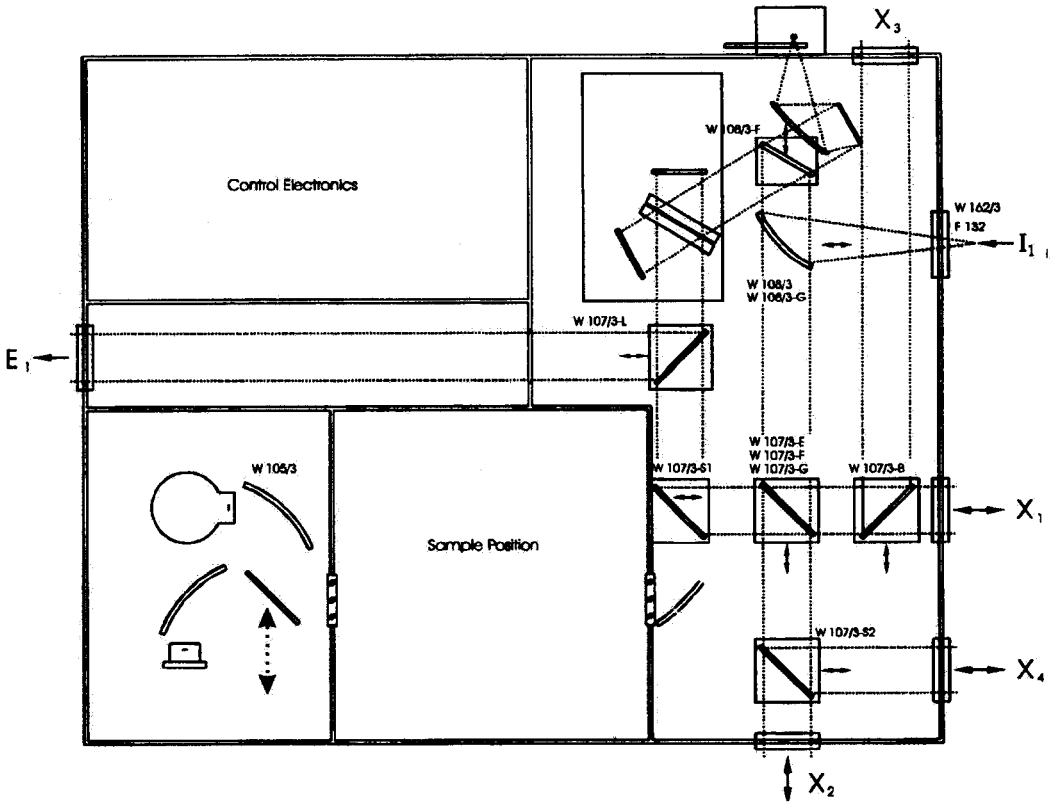

Alternative Optical Paths

	Description
I_1	Focused beam input - right side
E_1	Collimated beam output - left side
X_1	Collimated beam input or output -right side back
X_2	Collimated beam input or output - front
X_3	Collimated beam input or output - back
X_4	Collimated beam input or output - right side front

Figure 10: The standard optical path for the EQUINOX 55.

2.4.2 FT-IR experimental techniques

2.4.2.1 Transmission spectroscopy

The transmission spectroscopy (TS) technique is the oldest sampling technique in optical spectroscopy. In this technique, the sample is placed in the light beam of spectrometer and the intensity of the incident beam is compared with the intensity transmitted by sample.

For an incident beam of intensity I_0, the transmitted intensity I is given by

$$I = I_0 * 10^{-abc} \quad \text{.....(4)}$$

Where reflections are neglected

a = absorbtivity

b = sample thickness

c = concentration

There are few parameters that can be controlled in transmission spectroscopy and it is possible to adjust only the concentration and the thickness of the sample (Figure 11)

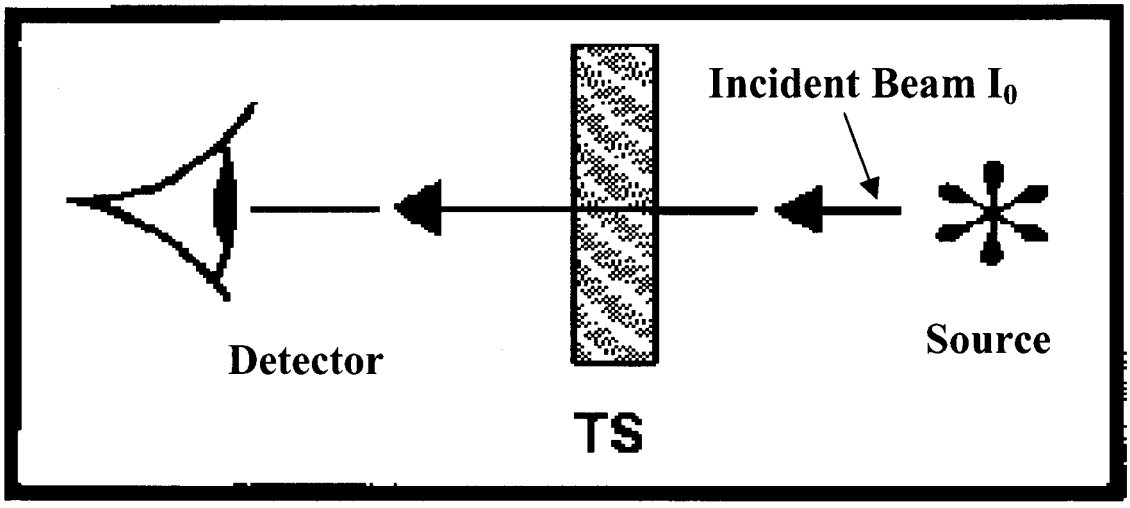

Figure 11: The transmission process and measurements.

2.4.2.1.1 Sample preparation

In contrast to most of other techniques, sample preparation for transmission spectroscopy is very important because usually the sample cannot be used "as is" and often, sample preparation is destructive of the sample. In all cases, the sample thickness must be adjusted, in some cases, a sample with smooth particles must be obtained and it should be imbedded in a matrix.

2.4.2.1.2 Solid samples

There are self-supporting materials such as films, rods and tapes, but it is necessary to mount the sample in a suitable frame that can be inserted into the slide holder in the sampling compartment. These frames can easily be made and care should be taken to ensure that they do not block the incident beam. The beams must not bypass the sample; in this case masks are used. The sample is also holes free in order to get good spectra. A thickness up to 2 mm can be used for far IR and the near IR. It is also recommended to use thinner films (as low as 0.001 mm) if the materials under study have polar functionality (e.g., C-F, C-Cl, C=O, CONH). Without a thin film, a severe saturation from total absorption of the polar groups will occur and quantitative analysis will be difficult. Generally, the film thickness for the quantitative analysis can very between 0.001-1 mm depending on the above-mentioned conditions.

2.4.2.1.3 IR transparent matrixes (KBr, KCl, NaCl)

When a powdered sample must be studied by transmission without thermal treatment, it is usually diluted in IR transparent materials such as KBr. By this method,

any matrix –effect (i.e dependence of the absorption spectra of species on the medium in which it occurs) is minimized, in addition, with dilution of the concentration. Molecular interaction is less likely to take place and Beer's Law is applicable. To make an appropriate KBr pellet, a milligram of sample should be ground in a mortar or microball mill mixed with 300 mg dry KBr, and then reground, the particle size should be less than a 1/5 of a wavelength to suppress the scattering. Dryness is very important and the mixture should be reground again if necessary before pressing into a pellet. The concentration of sample should range from 0.01-0.5% (W/W) depending on the absorbing group in the sample. The mixture is pressed for several minutes between 8 to 20 tons/cm^2. The main disadvantage of the KBr is that it is hygroscopic. Samples in a liquid form and water insoluble can be dispersed between two KBr plates as in the case of DPS.

2.4.2.2 External reflection spectroscopy (ERS)

External reflection spectroscopy is, in general, a non-destructive sampling technique. The sample of interest is studied without alteration, an important advantage for many samples. It is only in certain cases where the surface is rough; polishing is advisable in such a case and if the reflectivity is low, working with large angles of incident where the reflectivity is high might be of helping. The Figure 12 presents the ERS process.

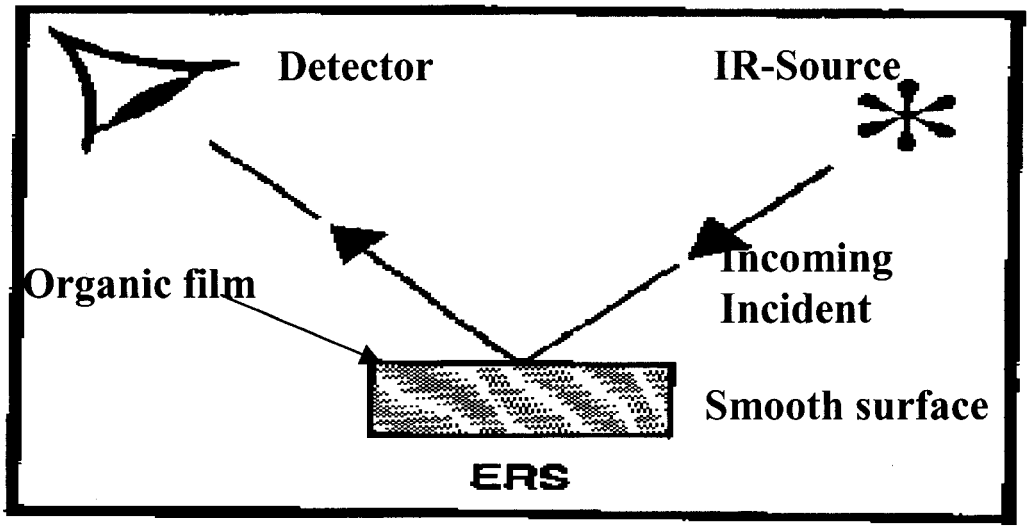

Figure 12: A diagram of the external reflection spectroscopy.

In ERS, the sample often consists of a film on a smooth metal surface. The films are usually formed and applied to the surface by different ways e.g, spinning, solvent casting, and vapor deposition. Because of the node that exists at near normal incident, high angles of incident usually between 70-89 degrees are chosen. The use of P-polarization increases the spectral sensitivity at this angle. Variable angle of reflection accessories can be used to determine the optimum angle for the particular system and to peak up the sensitivity. Unlike the internal reflection spectroscopy (IRS), in the ERS there are losses due to reflections, hence three to five reflections are considered an optimum number. ERS has been successfully used to study samples as thin as monolayer on metal surfaces. For thick films, ERS can be considered as double-transmission and sometimes referred to as Reflection Absorption Spectroscopy (RAS). The spectra can be detected at normal incident with either S or P polarization.

2.5 Evaporation system

2.5.1 Metal evaporation system

Vapour deposition is an outstanding technique for thin metallic film deposition for surface-enhanced Raman studies. Vacuum deposition has several advantages over other techniques that have been used to prepare a variety of thin films. It has control over the purity to some extent and temperature control during deposition. The utmost point to be considered is the uniformity of the arrival rate of the particles to the surface of the substrate, which gives the film its character. The deposition step is determined by both source and transport factors, together with conditions at the deposition surface.

There are three common factors that determine the structure and the composition of the surface, which are substrate surface conditions, roughness or smoothness in case of mirror as well as the level of contamination; reactivity of the surface with incoming materials and energy input to the surface mainly by the substrate temperature. It is necessary that all these parameters be considered for reproducible properties.

Monitoring of the rate and the thickness of the deposition is immensely important during the deposition process as it determines the property of the film. The most widely used technique to monitor the thickness of the thin film is the vibrating quartz method. This is a mass thickness method that employs a quartz crystal microbalance. For this research purpose, a XTC Inficon quartz crystal oscillator was used, which uses resonant crystalline quartz wafers. Crystalline quartz is piezoelectric, so a quartz wafer generates an oscillating voltage across itself when vibrating at its own resonant frequency. This voltage can be amplified and fed back to drive the crystal at this frequency. Electrical coupling is done with thin film metal electrode deposited on the opposite of a thin quartz

wafer having the proper crystallographic orientation. For deposition monitoring, one electrode is exposed to the vapor flux and proceeds to accumulate a mass of deposit. This mass loading reduces the crystal resonant frequency. A comparison of this frequency with that of the reference crystal, located in the instrument control unit, is used to calculate the mass deposit. The time derivative of the difference in frequency gives the evaporation rate.[82] A schematic of the vacuum evaporation system to prepare thin metal films is shown in Figure 13.

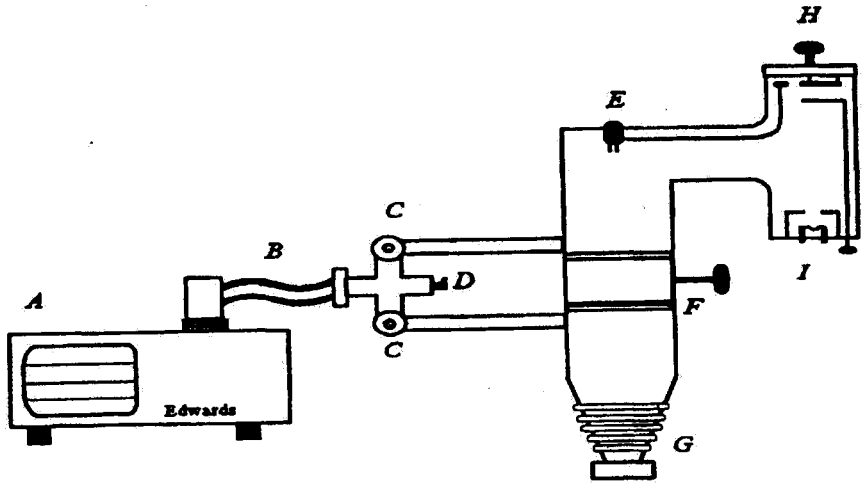

Key
- A Forepump
- B High Vacuum Connector Hose
- C Valves
- D Pressure Release Valve
- E Instrumentation Feedthrough: High Pressure Gauge, Deposition Rate Gauge
- F Butterfly Valve
- G Diffusion Pump
- H Lid: Substrate Table, thermocouple and heat Element Feedthroughs

Figure 13: The metal evaporator and its components.

2.5.2 Organic evaporation system (AUTO 306)

The Auto306 evaporation system is considered one of the most sophisticated physical vapor instruments used to coat the surfaces. It is fast and very efficient in controlling the rate of deposition at low rates. Wide ranges of accessories are available, which allow the configuration of the system for specific applications. Vacuum deposition at pressures as low as 10^{-7} torr can be achieved.

There are three major components from which the system is constructed, a pumping system, a baseplate, and an electrical system (which incorporates the Auto306 controller) (Figure 14). The pump system has a diffusion pump for high vacuum pumping and rotary pump for rough pumping and to support the diffusion pump. All the valves in the pumping system are electrically operated, under the control of the AUTO 306 controller (#3 in the sketch). The stainless steel baseplate (#1 in the sketch) has lead through holes for AUTO 306 roughing and pressure gauge pipelines and for accessory lead through. All the accessories that lead through holes are sealed with blanking plugs. The system is equipped with three circuit breakers, which protect the electrical supplies in the AUTO 306.

In this particular research, the system was used to evaporate 10 nm DPDS film onto a previously deposited 6 nm gold island film for SERS studies. The vacuum at the time of deposition was 10^{-6} torr and the rate of deposition was between 0.3 – 0.6 Å/s. The tooling factor was 92% and the Z-ratio was 0.1. The thickness of PTCDA film was 30 nm evaporated on smooth silver surface mirror with mass thickness of 90 nm for reflection absorption infrared spectroscopy (RAIRS) and the vacuum at the time of deposition was 5.0×10^{-7} torr. The DPDS RAIRS studies were carried out by depositing 25 nm of the

material on a 100 nm silver mirror and also by depositing 30 nm of DPDS on an aluminum mirror.

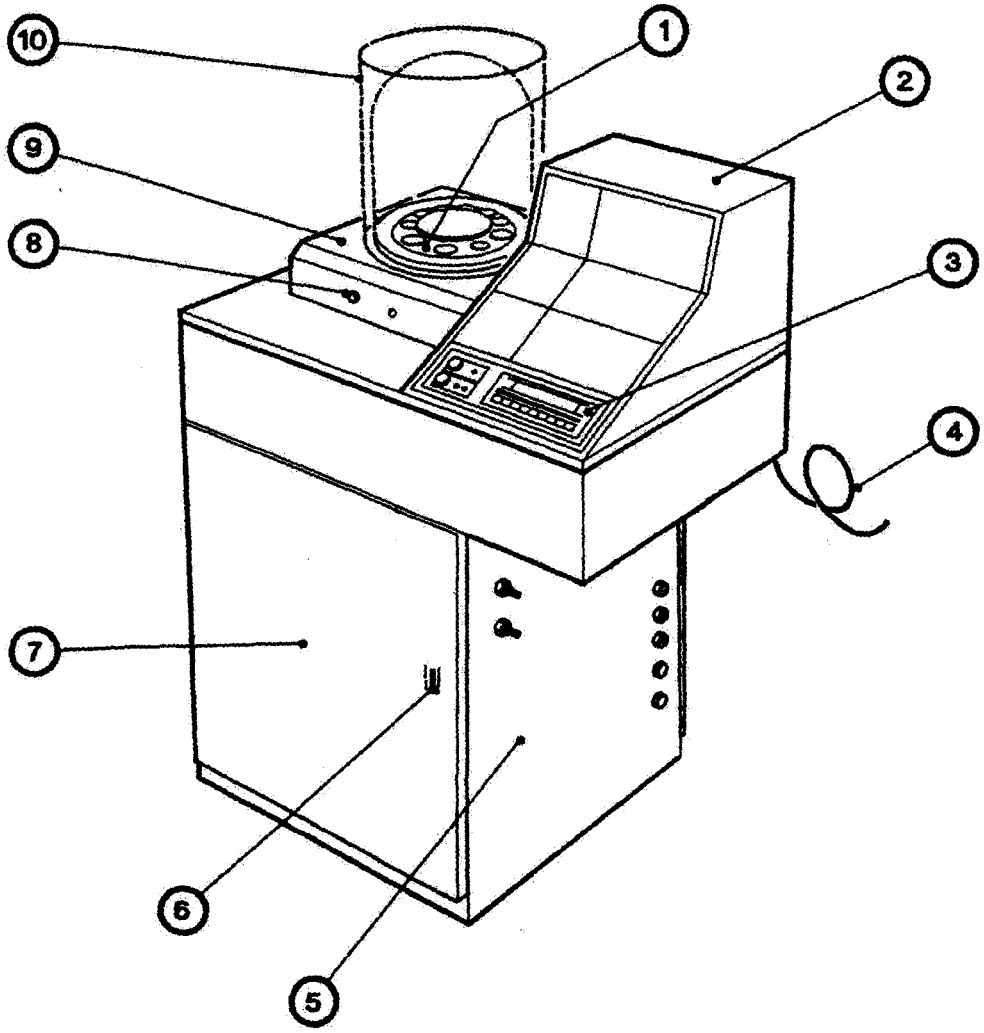

Key:				
	1	Baseplate	6	Front Door Lock
	2	Control cabinet	7	Front Door
	3	AUTO306 Controller	8	Needle Valve
	4	Electrical Supply Cable	9	Front Baseplate Bover
	5	Service Panel	10	Bell Jar and Implosion Guard

Figure 14: A modern Edward's AUTO 306 organic evaporator instrument and the main accessories.

2.6 UV-vis instrument

The UV-vis absorption spectra were routinely collected on the Varian 50 UV-vis single beam spectrophotometer. The instrument shown in Figure 15 is an example of a temporal dispersive instrument and operates via a sequential linear scan. It contains a continuous xenon lamp light source that flashes only when acquiring data point thereby preventing photo degradation of photosensitive samples and allowing a collection rate of 80 data points per second. The wavelength detector consists of a monochrometer with a motor driven reflecting grating system that sweeps the spectral region of interest at a constant rate. A photoelectric detector enables the detection of the radiant energy and the detection is synchronized with the motion of the grating allowing a wavelength scale based upon time to be recorded. A beam splitter is employed to enable simultaneous reference beam correction. The spectral rang is 190-1100 nm. Data acquisition is performed on the Cary WinUV software for windows, while data is manipulated using the Galactic Industries GRAMS/32^{TM} C software.

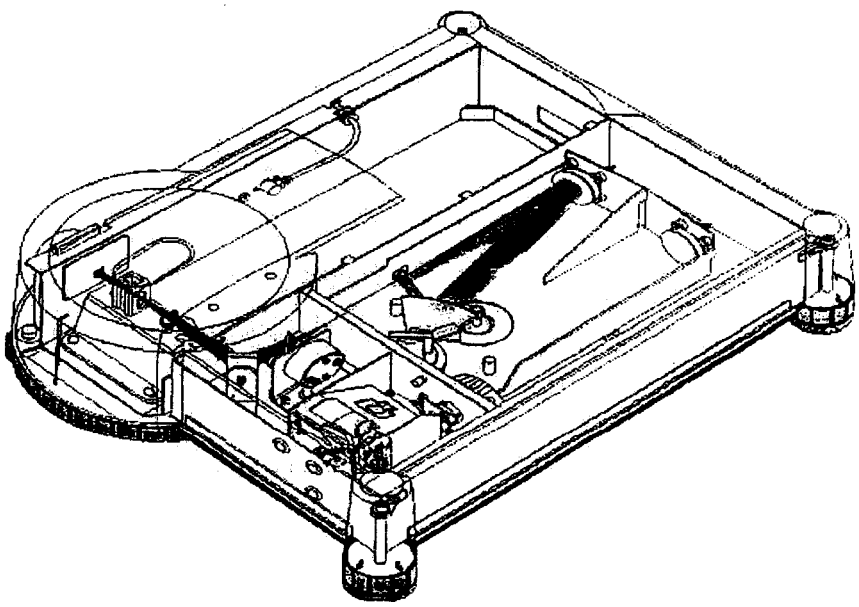

Figure 15: The Cary 50 UV-vis spectrometer.

3. DIPHENYL DISULFIDE AND DIPHENYL SULFIDE

3.1 Diphenyl disulfide

3.1.1 Electronic spectra

Diphenyl disulfide is a white powder, soluble in methanol and its molecular structure has two phenyl groups and two sulfur atoms as shown in Figure 16. The solution of the DPDS in methanol is colorless; it does not absorb in the visible region, and shows a very weak absorption in the ultraviolet. The electronic spectrum given in Figure 17 shows the UV-vis absorption of 10^{-3} M of DPDS solution in methanol. Two absorption bands were seen at 275 and 278 nm. The activity is likely due to $\pi \rightarrow \pi^*$ transition, the energy for unconjugated double bond is much higher and about 7 eV. The presence of conjugated double bond will shift the absorption to the longer wavelength.[83]

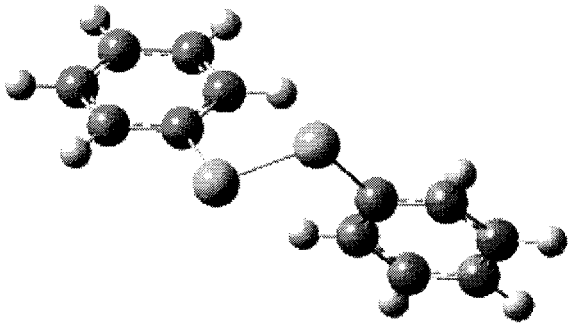

Figure 16: The optimized geometry of DPDS.

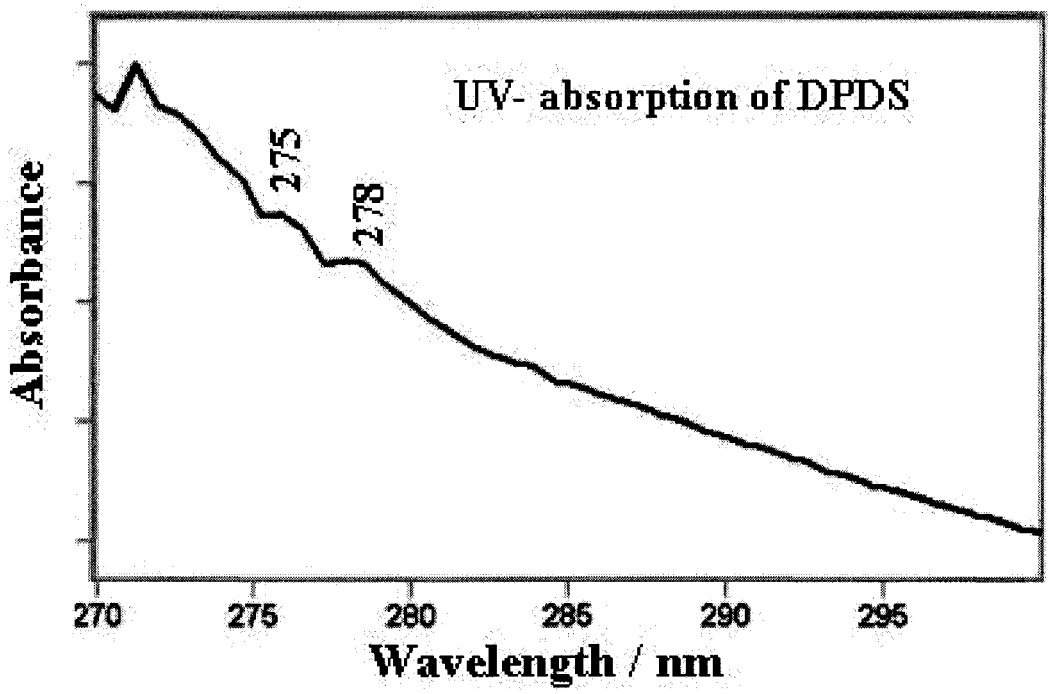

Figure 17: UV absorption spectrum of 10^{-3} M DPDS solution in methanol.

3.1.2 Surface-enhanced Raman scattering of DPDS

3.1.2.1 Theoretical calculations

The *ab initio* geometry optimization for DPDS at the B3LYP at 6-31G* level of theory was carried out by Marti[84] to present a UV-vis and IR characterization study of DPDS. Since the final aim of the latter report was not the vibrational analysis, the Raman spectra was not computed and only the relevant part of the IR spectra was discussed. The minimized geometry of DPDS given a molecular structure with a C_1 point group and 66 (3N-6, N=24) vibrational degrees of freedom is shown in Figure 16 for what all of the vibrational modes are allowed in infrared and Raman. The computed minimum energy is E = -1259.677 a.u. and dipole moment of 1.9185 D. The dihedral angle C-S-S-C was found to be 94.4° a bit larger than in the previous computation. The S-S bond distance is at 2.06 Å and the C-S is 1.80 Å. The minimized geometry produces a set of positive

vibrational wavenumbers with 66 vibrational fundamentals. There are 25 stretching vibrations and 41 bending and dihedral internal coordinates. The 25 stretching modes, 10 are C-H stretches at high frequency and two are ring-breathing modes of the benzene rings. The remaining 13 stretching modes correspond to: one S-S stretch, two C-S stretches and 10 benzene ring stretching modes. The modes are linear combinations and some of them, in the 1000-1600 cm^{-1} region, contain large contributions from C-H bending as shown in Table 1, the complete vibrational assignment for the DPDS molecule including SERS results on colloidal silver is given (Raman and SERS on silver colloids with different excitations). The experimental results were aided by theoretical calculation of the two molecules using Density Functional Theory (DFT) B3LYP at 6-31G (d) level.[85] The calculated S-S vibrational fundamentals was assigned at 502 cm^{-1} using Gauss view software for Windows, it was the first time this band was assigned with the help of theoretical approximation for this particular molecule, the relative intensity of the band was taking into account when assigned. Table 2 shows the rest of the SERS investigation and studies on different substrates, which are silver and gold island films. From the spectra it can be concluded that the S-S bond cleaves on the rough metal surfaces and is not observed in the SERS spectra on different substrates. Calculated and experimental (powder) Raman spectra are presented in Figure 18, since there is no absorption in the visible, the Raman spectra obtained with the 514.5 nm, 633 nm and 780 nm are identical. There is a good agreement between the observed and experimentally measured spectra. The inset shows a unique agreement at higher vibrational frequencies.

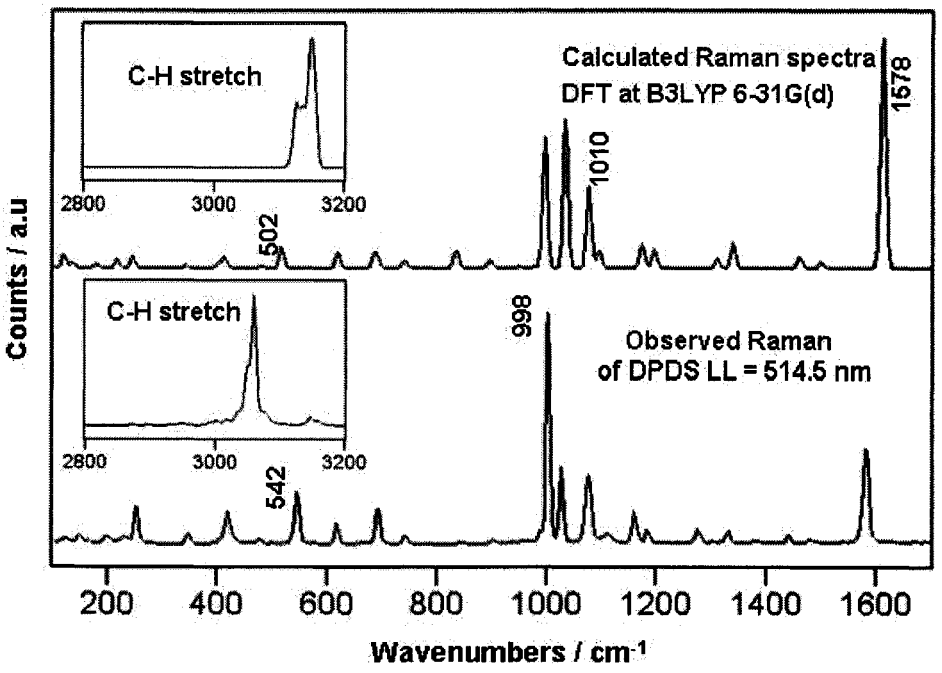

Figure 18: The comparison between observed and calculated Raman spectra of DPDS using DFT at B3LYP/6-31G(d) level.

It should be pointed out that the observed spectra are for solid samples, where there are condensed phase effects that may strongly affect the relative intensity of the vibrational bands. A case in point are the C-H stretching vibrations where the computed strong Raman intensities correlate with the observation, while the observed relative intensities of the C-H in the infrared spectrum are much lower than the calculated integrated intensities as it will be shown latter. The calculated Raman intensities were normalized to the most intensive band at 3093 cm^{-1}. All the vibrational fundamentals were assigned using a Gauss view program.

Table 1 Observed SERS on Ag colloids and calculated fundamental vibrational wavenumbers of DPDS. *Scaling factor 0.9614.

Calculated Frequency*	Raman Intensities	Neat Raman 514nm	SERS on Ag colloids			Assignments
			514nm	633nm	780nm	
3093	100	3057	3056	3057		C-H str.
3091	15					C-H str.
3087	83					C-H str.
3086	14					C-H str.
3076	42					C-H str.
3075	21					C-H str.
3066	34					C-H str.
3066	34					C-H str.
3061	5.0					C-H str.
3060	7.0					C-H str.
1580	17					C=C str.
1578	18	1577	1572	1571	1574	C=C str.
1572	3.0					C=C str.
1571	1.0					C=C str.
1468	1.0	1481	1470	1471	1476	Ring str.
1467	0.0					Ring str.
1429	1.0	1439				Ring str.+C-H bending
1428	0.0	1380	1380			Ring str.+C-H bending
1311	4.0	1327				Ring str.
1308	0.0	1297				Ring str.
1281	1.0	1274				Ring str.
1278	0.0					Ring str.
1170	2.0	1179	1178	1177		C-H bending
1168	1.0					C-H bending
1146	3.0	1158				C-H bending
1146	1.0					C-H bending
1070	2.0	1105	1105	1107	1100	Ring str.+C-H bending
1069	0.0					Ring str.+C-H bending
1055	13	1073	1071	1070	1070	Ring str.+C-H bending.
1051	11					Ring str.+C-H bending.
1010	20	1023	1020	1018	1020	Ring str.
1009	3.0					Ring str.
972	17	998	997	997	998	Ring breath

Calculated Frequency*	Raman Intensities	Neat Raman 514 nm	SERS on Ag colloids 514 nm	633 nm	780 nm	Assignments
972						Ring breath
955	0.0					C-H bending
954	0.0					C-H bending
929	0.0					C-H wag.
927	0.0					C-H wag.
875	1.0	900				C-H wag.
871	0.0					C-H wag.
816	2.0	841				C-H wag.
811						C-H wag.
723						C-H wag.
722						C-H wag.
676	0.0	690	690	688	688	C-C-C bend.
672	0.0	688				C-C-C bend.
670	1.0	684				C-C-C bend.
669	1.0					C-C-C bend.
605	2.0	616		615		Ring def. + C-S str.
603	0.0					Ring def.
502	3.0	542				S-S str.
466	0.0	474		467		Ring def.
462	0.0					Ring def.
401	1.0	415	415	416	415	Ring def.+ C-H bend
399	0.0					Ring def.
395	0.0					Ring def.
388	0.0					Ring def.
331	0.0	334				Skeletal def.
236	1.0	246				Skeletal def.
209	1.0					C-SS-C def.
173	0.0	228				C-SS-C def.
129	1.0	173				Skeletal def.
114	2.0	145				Ring wag.
44	3.0	118				Ring wag.
22	3.0					Ring wag.
11	1.0					Ring wag.

3.1.2.2 Surface enhanced Raman scattering of DPDS on silver colloids and films

The surface plasmon absorption for silver colloids, silver evaporated films and gold evaporated films used as active substrates for SERS are shown in Figure 19.

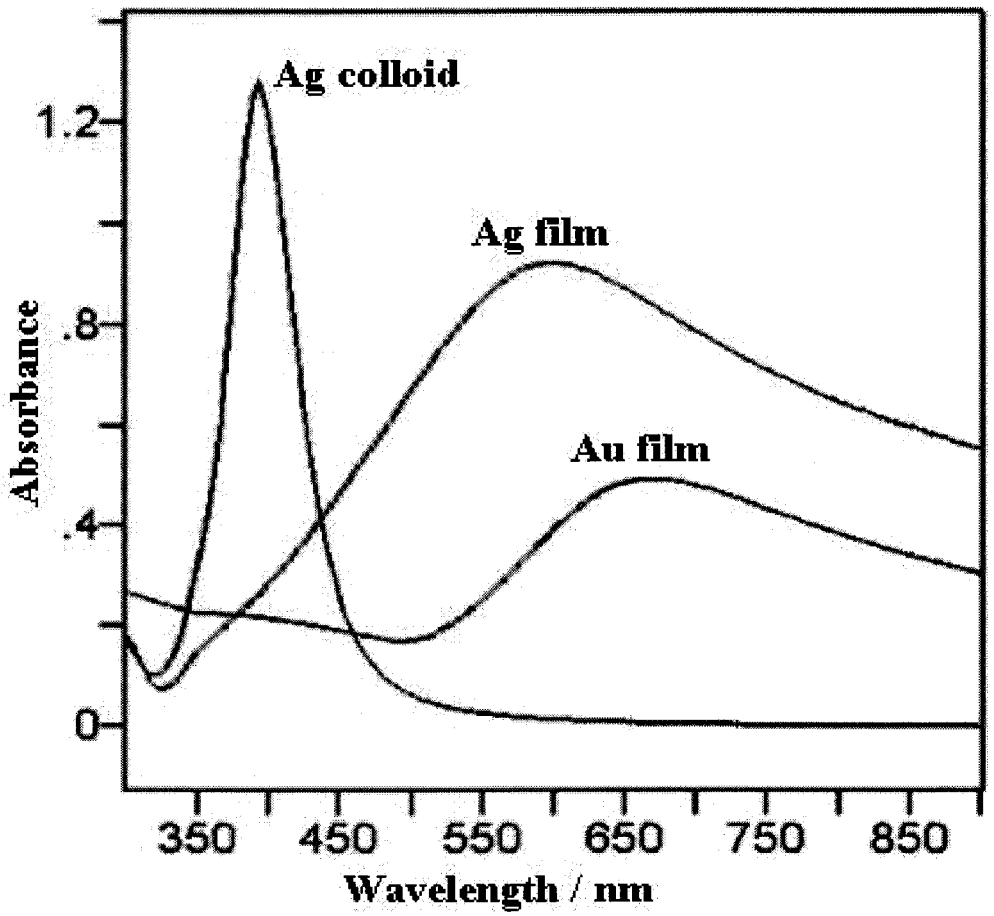

Figure 19: Plasmon resonances of evaporated silver film, gold film and silver colloids.

DPDS 10^{-3} M was prepared in methanol and 10 microliter droplet of the solution was used for the casting on 6 nm silver films. It was observed that the DPDS adheres and dries very fast on silver substrate leaving no room for bulk organic film to be formed. 50 microliters of DPDS solution was added to the 3 ml of the colloidal silver because the addition of 100 microliters shows the collapsing of the DPDS–silver into an aggregated colloid. To illustrate the spectra obtained for neat DPDS and that of SERS of DPDS adsorbed on a 6 nm silver film excited with lower laser power (780 nm). Figure 20 shows both spectra. The most important features are marked in the spectra. The vibrational band at 542 cm^{-1}, assigned to the S-S stretching vibration in the DPDS solid, is not present in

the SERS spectrum, confirming the cleavage of the S-S bond. Excitation with the 780 nm line, or any other higher energy laser line, shows that the S-S bond breaks on the rough surfaces. The cleavage of the DPDS is observed with the same characteristics on silver colloids with all three-laser lines: 514.5 nm, 633 nm and 780 nm. The S-S stretch is calculated at 502 cm^{-1} after scaling down from 524 cm^{-1} and carries an intensity value that is about 1/6 of the value of the ring stretching at 1010 cm^{-1} (in agreement with the observed spectrum shown in Figure 18). The SERS spectrum of DPDS corresponds exactly with the SERS spectrum of thiophenol on silver.[43] However, the Ag-S stretching vibration is not clearly detected as can be seen in Figure 20. The 246 cm^{-1} peak in the neat spectra is marked to highlight the absence of a SERS band in the spectral region where the Ag-S would be found: 237 cm^{-1} is the value quoted by Kim et al..[43]

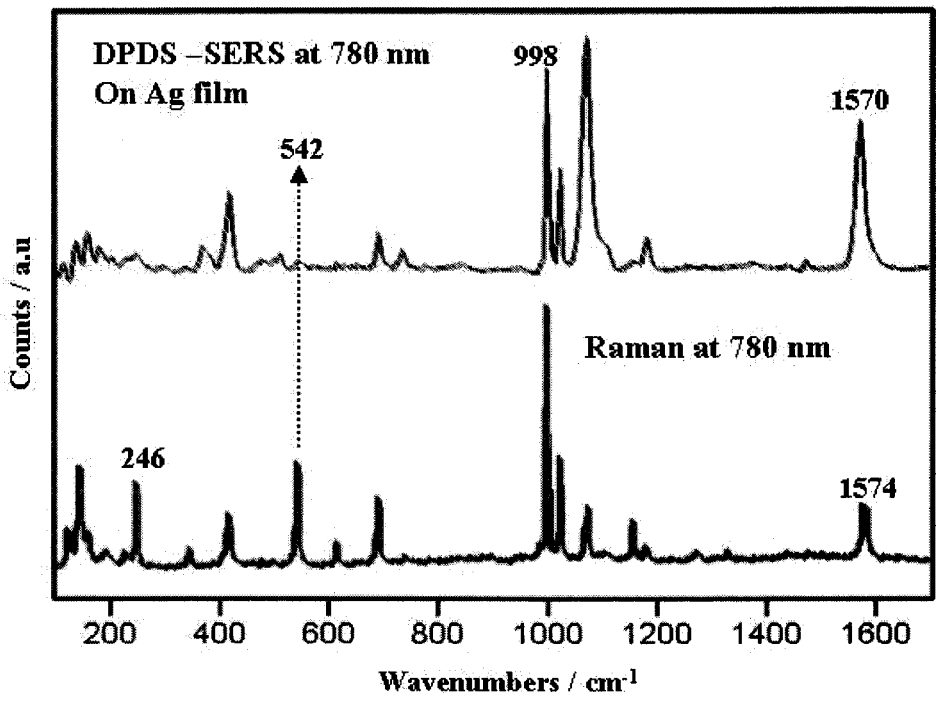

Figure 20: Observed and SERS spectrum of DPDS cast on a silver film.

The spectra on silver colloids, obtained with the 633 nm and 514.5 nm laser lines are shown in Figure 21. The other technique was to prepare another active substrate represented in gold island films. SERS on gold film was obtained by physical evaporation of DPDS using Auto 306 evaporation systems, vacuum evaporation of 10 nm mass thickness of DPDS onto a 6 nm gold film. Using the 633 nm line, the cleavage is readily observed on gold island film with exactly the same products as on silver as can be seen in Figure 21. Since the spectrum corresponds to that of the thiophenolate, the metal oxidation must occur in the solid-state reaction of the DPDS with gold with the corresponding reduction of the DPDS to a sulfide. It was concluded that the cleavage might happen as the band at 542 cm^{-1} disappears from the SERS spectra of DPDS regardless the excitation energy and rough surface used. However, it was possible to observe clearly the Ag-S or Au-S band at lower frequency in any of SERS spectra.

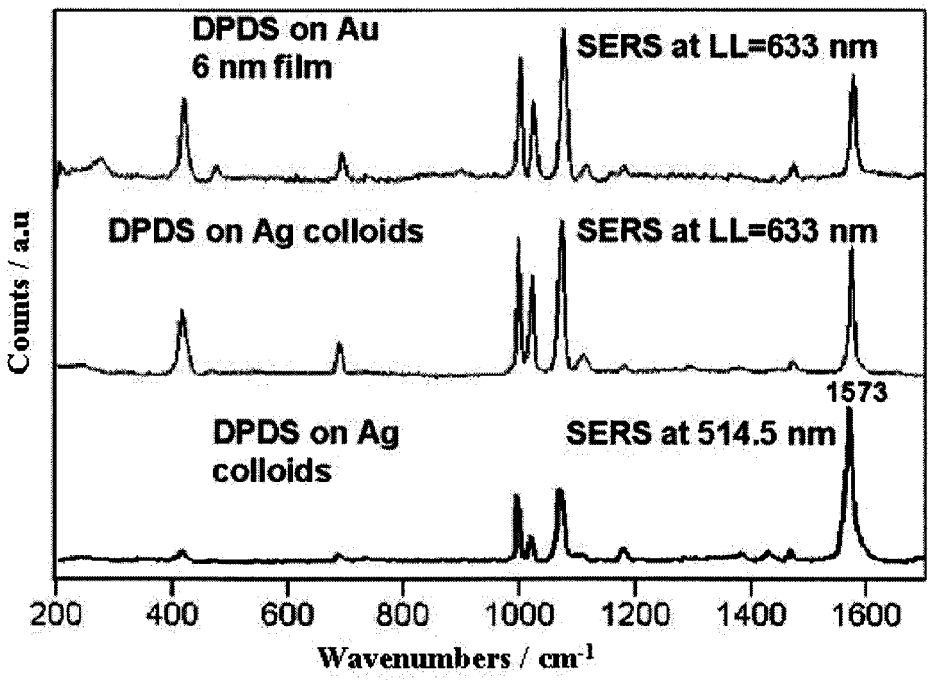

Figure 21: SERS spectra of DPDS on silver colloids and a gold island film.

The SERS spectra obtained from the DPDS dissociation have the peculiar property of low enhancement factors. This is in contrast with the large enhancement factor observed for dialkyl sulfides[18], where there is no cleavage of the C-S bond, and no chemical reaction with the metal surface. Low enhancement factors, and the absence of the metal-S stretching vibration or unclear observation, may be the consequence of a strong chemical reaction with the surface that destroys the surface nanostructures responsible for high average enhancement factors in SERS.[86]

Table 2 Observed SERS on Ag/Au films and calculated fundamentals vibrational wavenumbers of DPDS.

Calculated Frequency	Raman Int.	Neat Raman	Cast Colloids	Ag film 514.5nm	Ag film 633nm	Ag film 780 nm	Au film 633 nm
3093	100	3057	3057	3057	3057		3059
3091	15						
3087	83						
3086	14						
3076	42						
3075	21						
3066	34						
3066	34						
3061	5.0						
3060	7.0						
1580	17						
1578	18	1577	1571	1573	1573	1572	1574
1572	0.0						
1571	0.0						
1468	1.0	1481	1471	1472	1473	1473	1472
1467	0.0						
1429	1.0	1439		1451	1452		1441
1428	0.0	1380		1380	1380	1380	
1311	4.0	1327					
1308	0.0	1297		1290	1291		
1281	1.0	1274			1281	1274	
1278	0.0						
1170	2.0	1179	1177	1181	1180	1181	1180
1168	1.0						

Calculated Frequency	Raman Int.	Neat Raman	Cast Colloids	Ag film 514.5nm	Ag film 633nm	Ag film 780 nm	Au film 633 nm
1146	3.0	1158		1156	1159	1156	
1146	0.0						
1070	2.0	1105	1107	1108	1108	1106	1115
1069	0.0						
1055	13	1073	1070	1074	1072	1070	1075
1051	11						
1010	20	1023	1018	1020	1021	1021	1023
1009	0.0						
972	17	998	997	997	999	998	999
972	0.0						
955	0.0						
954	0.0						
929	0.0						
927	0.0						
875	0.0						
871	0.0						
816	2.0	841			851	851	
811	1.0			836	834	836	
723	1.0	740		798	800	801	
722	0.0						
676	0.0	690	688	689	690	689	694
672	0.0	688					
670	0.0						
669	0.0						
605	2.0	616	615	614	615	614	618
603	0.0						
502	3.0	542					
466	0.0	474	467	467	471	470	476
462	0.0						
401	1.0	415	416	416	417	416	416
399	0.0						
395	0.0						
388	0.0						
331	0.0	0.0					
236	1.0	246					
209	0.0						
173	0.0	228			161	160	
129	1.0	173					
114	2.0	145					
44	3.0	118					
22	3.0						
11	1.0						

3.1.2.3 Metal-sulfur complex (Ag-S)

The Ag-S bond is considered to be the driving force in the adsorption of mercaptophenols; one challenging point in this work was the precise determination of the lower frequency band of the Ag-S stretching vibration. The band assignment is based on the Raman spectra taken from a salt complex of DPDS. The preparation was simple, 1:1(by volume) solutions of both silver nitrate dissolved in water and DPDS in methanol with same concentrations of 10^{-3} M were added, and a white deposit was instantly formed, filtered and left to dry under vacuum. However, the Ag-S stretching vibrational band was not clearly seen in the SERS spectra. Our own previous study of P-nitrothiophenol showed indirect evidence of the silver complex, but the Ag-S stretch was not identified.[70] Kim[40] has also studied the SERS of 1,2-benzenedithiol adsorbed on silver and reported a weak shoulder at 262 cm^{-1} to be assigned to the Ag-S stretching vibration where both sulfur atoms are attached to the surface. A SERS study of the 1,4-benzenedithiol adsorbed on silver[87] also provides evidence of chemisorption through an Ag-S bond, however the Ag-S stretch is not seen. That is partly explained by a possible face-on molecular orientation. Since the formation of a metal-sulfur bond is indirectly confirmed in all the studies involving copper, silver and gold, it is helpful to remember the spectral region where the stretching vibration of the metal sulfur bond is observed. In a series of alkane and arene-monothiolate complexes it was found that the spectral region for the Cu-S stretching vibration should be within 150-250 cm^{-1}, and the corresponding vibration for the Ag-S bond is in the 140-210 cm^{-1} region.[88] The Ag-S bond is widely accepted as central to the formation of self-assembled monolayers on silver[89] and gold surfaces.[90] However, the detection of the metal-sulfur bond remains elusive in the

vibrational spectra of self-assembled monolayers. In the past publications, almost all of the Ag-S vibrational assignments depend upon the less intensive bands in the lower frequency region. In our case, a prepared sample powder of the salt was grinded on the glass slide (smoothening the crystals) and 514.5 nm laser was the excitation line and the resulted spectrum is seen in Figure 22. It was found that a very weak shoulder at 244 cm^{-1} of a weak band could safely be assigned for Ag-S stretching vibration; the inset shows clear evidence. The Ag-S stretching band intensity is presumably too weak to be observable in the SERS spectra and possess a weak scattering intensity.[91]

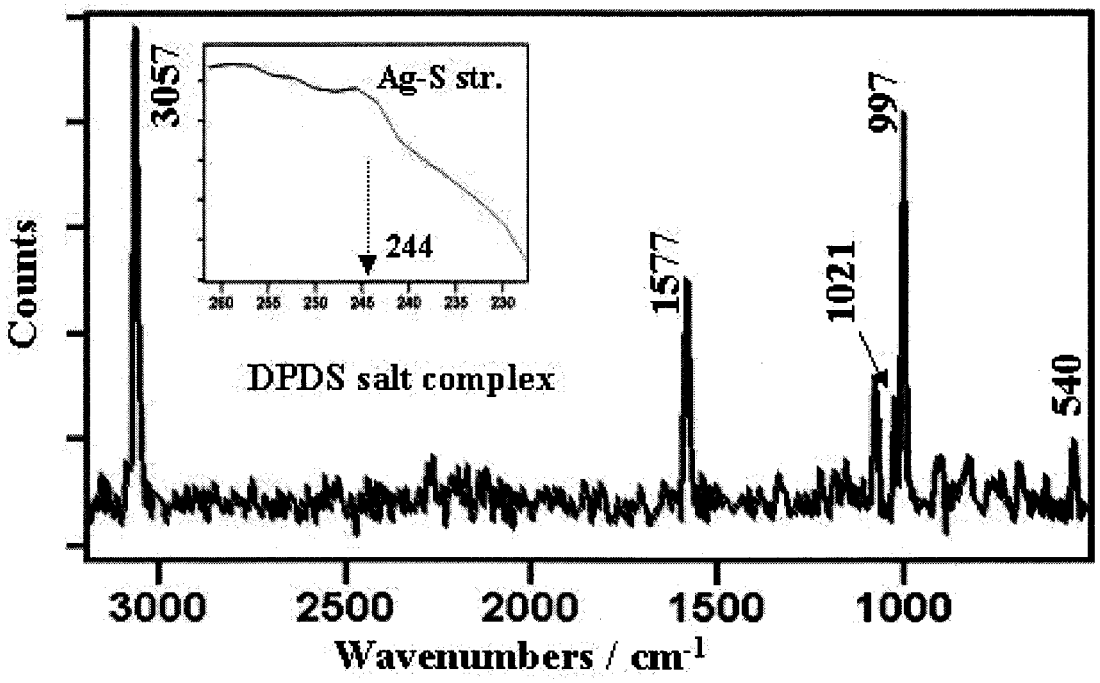

Figure 22: Raman spectrum of Ag-DPDS salt complex using 514.5 nm excitation.

3.1.3 FT-IR studies of DPDS

3.1.3.1 Transmission spectra

The vibrational assignment of DPDS was helped by using *ab initio* theoretical computations of frequencies and intensities. The FT-IR studies included the transmission and reflection absorption infrared spectroscopy (RAIRS) concepts, which complement each other especially regarding the study of the molecular orientation. Transmission FT-IR spectra of DPDS dispersed in a KBr pellet (transparent substrate) is shown in Figure 23. The agreement between the experimental spectra with theoretically calculated spectra is very good, even with respect to most relative intensities of the vibrational modes, except the C-H stretching modes. The observed relative intensities of the C-H in the infrared spectrum are much lower than the calculated integrated intensities and that might be due to the condensed phase effect.

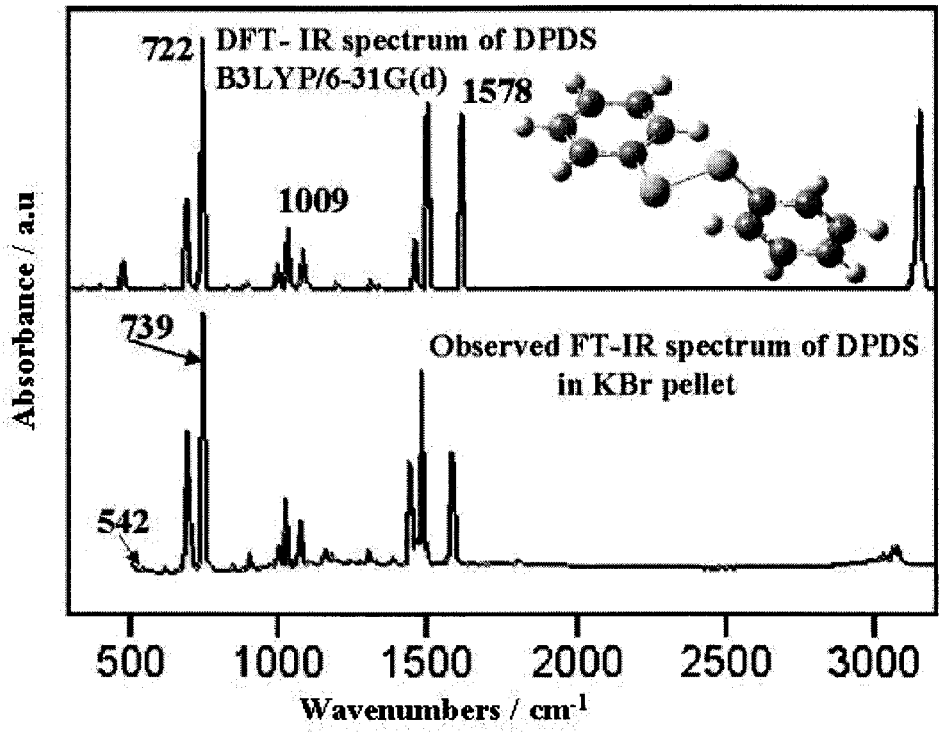

Figure 23: Observed and calculated infrared spectra of DPDS.

Table 3 Observed and calculated FT-IR vibrational fundamentals of DPDS.

Calculated frequency (cm^{-1})	Normalized Intensity	Observed FT-IR (cm^{-1})	Normalized Intensity	RAIRS
3093	13			
3091	13			
3087	5.0			
3086	79	3070	4.0	
3076	32	3056	4.0	
3075	29	3026	2.0	
3066	2.0			
3066	2.0			
3061	3.0			
3060	2.0			
1580	15			
1578	82	1576	28	
1572	0.0			
1571	0.0			
1468	21			
1467	80	1475	49	
1429	9.0	1454	6.0	
1428	19	1437	26	
1311	0.0	1384	1.0	
1308	2.0	1327	0.6	
1281	2.0	1298	3.0	
1278	3.0	1274	1.0	
1170	0.0			
1168	3.0	1178	2.0	
1146	0.0	1154	3.0	
1146	0.0			
1070	4.0	1100	4.0	
1069	0.0			
1055	19	1072	10	
1051	0.0			
1010	0.0			
1009	27	1022	16	
972	13	996	5.0	
972	0.0			
955	0.0	984	2.0	
954	0.0	967	0.0	
929	0.0			
927	0.0			
875	0.0	900	2.0	
871	0.0	844	0.0	844
816	0.0			

Calculated frequency (cm^{-1})	Normalized Intensity	Observed FT-IR (cm^{-1})	Normalized Intensity	RAIRS
811	0.0			
723	44			
722	100	739	100	
676	15			
672	20			
670	23	688	33	
669	0.0			
605	0.0			
603	0.0	613	0.0	
502	0.0	542	0.0	542
466				
462				
401				
399				
395				
388				
331				
236				
209				
173				
129				
114				
44				
22				
11				

3.1.3.2 Reflection absorption infrared spectroscopy (RAIRS)

The RAIRS is a technique, which is widely used to characterize a thin film and to help with the finding of molecular orientation. The RAIRS is sometimes called an external reflection spectroscopy (ERS), when light is reflected from smooth surface (metal, semiconductor, or liquid). It was Greenler who investigated not only the experimental[92] but also theoretical[93] conditions to produce the highest absorption in the single reflection technique. He also considered[93] the effect of the molecular orientation with respect to the metal surface. A single reflection is sufficient for obtaining a good RAIRS spectrum[94] and indeed the single reflection is used in RAIRS experiments. It is

the interaction of the electromagnetic radiation with the oscillation dipole associated with particular normal vibrational modes that allows the vibrational excitation of molecules in both the bulk and the adsorbed phase. Metals are highly reflective in the infrared. The incident and reflected beam and the surface normal lie in the so-called plane of incidence as shown in Figure 24. The interaction of the light with the surface is described by Fresnel[95], which incorporates the appropriate boundary conditions in the electromagnetic wave equations of the incident, reflected and refracted wave fronts, providing an amplitude and phase of the reflected waves with respect to the incident in terms of the complex index of refraction of the phase making up the interface. The amplitude and phase changes experienced in reflection depend upon the direction of the electric field vector of the wave fronts, and it is convenient to resolve the electric field vector into components in the incident plane (P Polarized) and normal to the incident plane (S polarized) Figure 24.

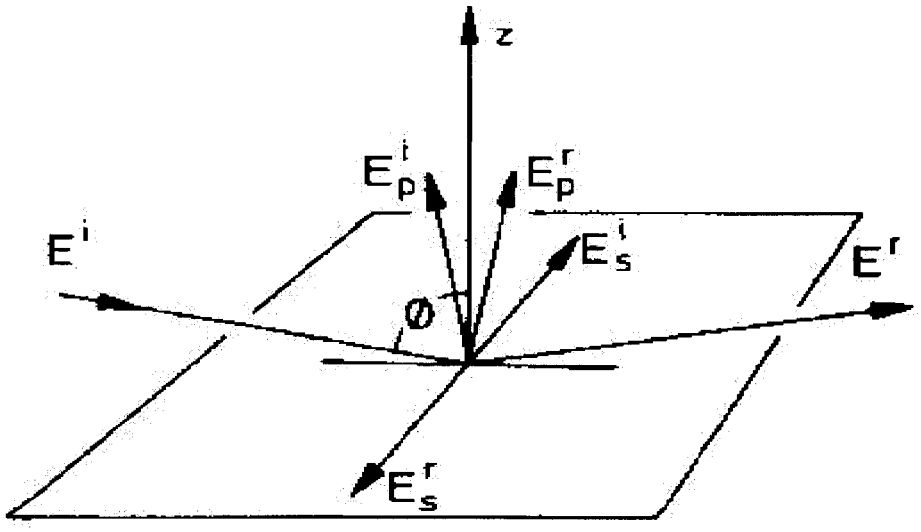

Figure 24: Reflection geometry showing the S and P components of the electric field of incident (E^i) and reflected (E^r).

3.1.3.3 Reflection absorption infrared spectroscopy (RAIRS) of DPDS

The RAIRS experiment is ideally designed to obtain the vibrational absorption spectrum from very small number of adsorbed molecules on a single crystal metal surface in single reflection. In addition to the study of the breakage of the DPDS on rough surfaces, the conformation and the orientation of the DPDS on smooth surfaces can also be studied by means of reflection absorption infrared spectroscopy (external reflection). As it is noticed in the experimental section, there were two different techniques of FT-IR instrumentation used to obtain RAIRS spectra of DPDS and the resulted spectra were identical. Moreover, the collected RAIRS of DPDS was compared with the transmission spectra of diphenyl disulfide to investigate the orientation of the molecule on metals.[96] The RAIRS spectra were collected using two different reflecting substrates. A 100 nm mass thickness forms smooth metal surfaces of silver and aluminum. The mirrors were covered with a 25 nm film of DPDS. An Edwards Auto 306 evaporator was used to deposit the desired film thickness; with a rate of the deposition of 0.3-0.6 Å/s and the background pressure during the deposition was 5×10^{-7} torr. The aluminum was used just to eliminate the possibility of high reactivity of silver surface with the adsorbate. Identical RAIRS spectra were obtained. Greenler stated that the light at reflecting smooth surface is highly polarized, and at certain angle of incident the P-polarized component of the electromagnetic wave is three orders of magnitude greater than S-polarized or the parallel component. A close look of the transmission and reflection spectra of DPDS, shows that the band at 844 cm^{-1}, assigned for C-H wagging, Table 3, becomes more intense compare with its relative intensity in the transmission spectra. It is clear that the P-component of the electromagnetic radiation of the IR interacts with C-H wagging. As

the band becomes more intense in RAIRS, it can be concluded that one of the DPDS rings sits flat or face-on on the surface regardless the breakage. Only a few bands are seen in the RAIRS. However, the S-S stretching vibration can be seen in the inset of the Figure 25. The appearance of the S-S bond in the RAIRS proves that the DPDS might not cleave on the smooth metal surfaces, and adsorb with only one sulfur atom.

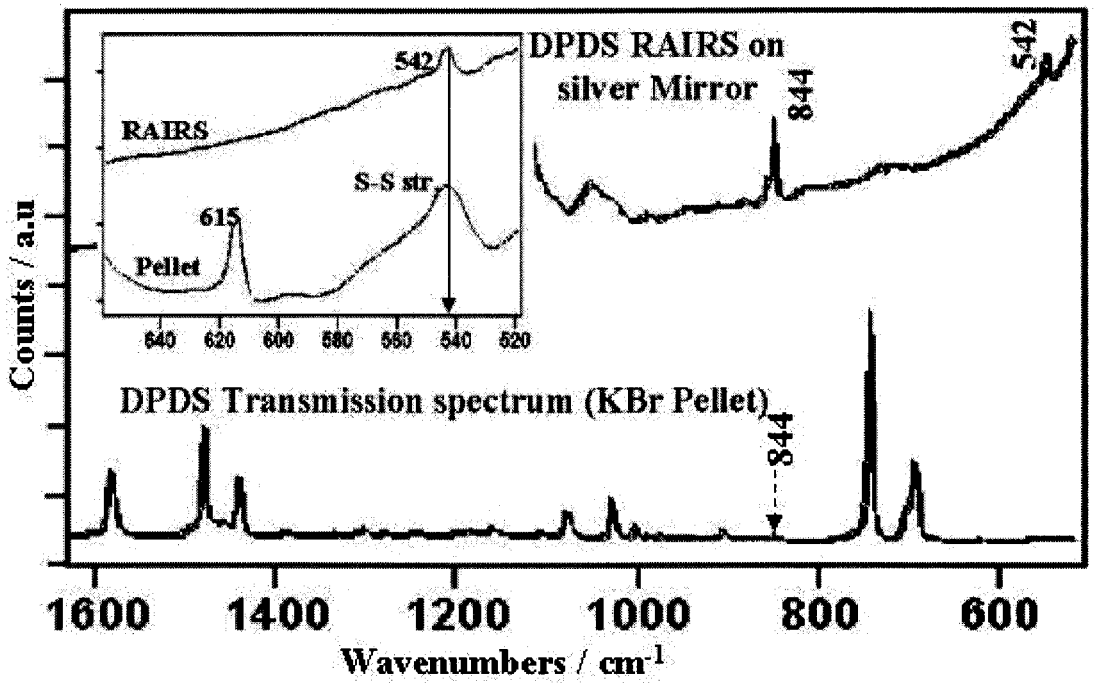

Figure 25: RAIRS and transmission spectra of DPDS revealing the orientation of adsorbed molecule.

3.2 Diphenyl sulfide (DPS)

A complete study of the diphenyl sulfide (DPS) was also carried out. The assignment was aided with a DFT computation B3LYP at 6-31G (d) basis set and SERS spectra were obtained with the three laser lines on silver and gold colloids and silver evaporated films. DPS is not a planar molecule (minimized geometry) with C_1 symmetry point and 63 fundamental vibrations. All vibrational fundamentals are Raman and

infrared active. The minimized geometry with E = -861.561 a.u. and a dipole moment of 1.6157 D is shown in Figure 26. Notably, the calculated C-S stretching vibrations are below 700 cm^{-1}. The observed Raman and SERS wavenumbers for DPS in colloidal silver solution collected using different excitation lines (514 nm, 633 nm, and 780 nm) for solid DPS, as well as the results of the *ab-initio* calculations are listed in Table 4. The observed Raman spectrum of solid DPS and the calculated Raman intensities are shown in Figure 27. Despite the fact that the computed spectrum should be compared with gas-phase spectrum, it can be seen that the intensity patterns in these two spectra are in reasonable agreement. The calculated DPS and observed FT-IR spectra of DPS are presented in Figure 28, which shows that the two spectra are in a good agreement. It is important to point out that the Raman spectra recorded with laser lines at 514.5 nm, 633 nm and 780 nm should be identical, in agreement with the fact that excitation frequencies are far from the electronic absorption band.[97]

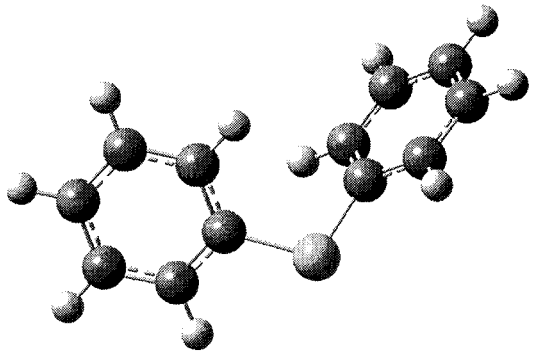

Figure 26: The minimized geometry of DPS.

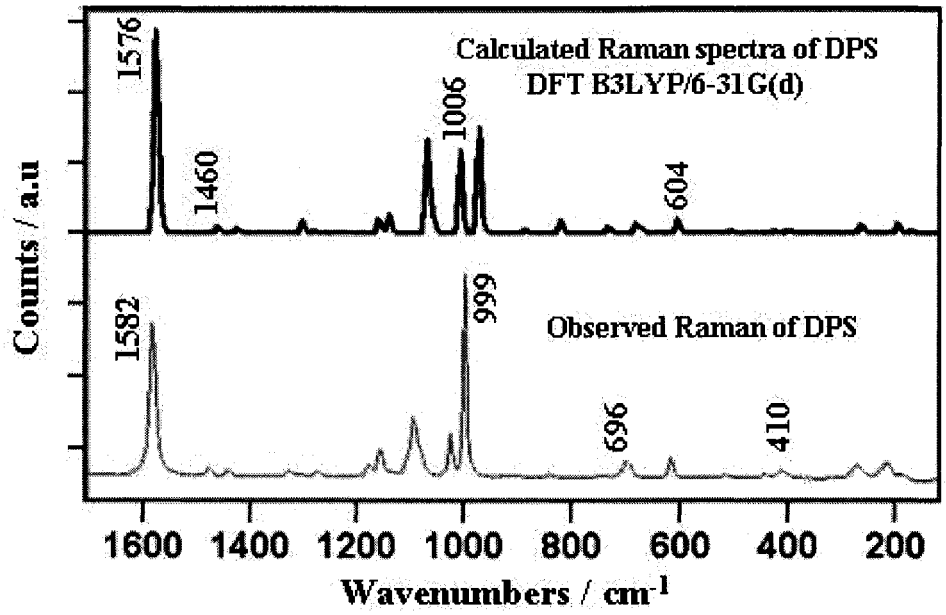

Figure 27: Calculated and experimental Raman spectra of DPS.

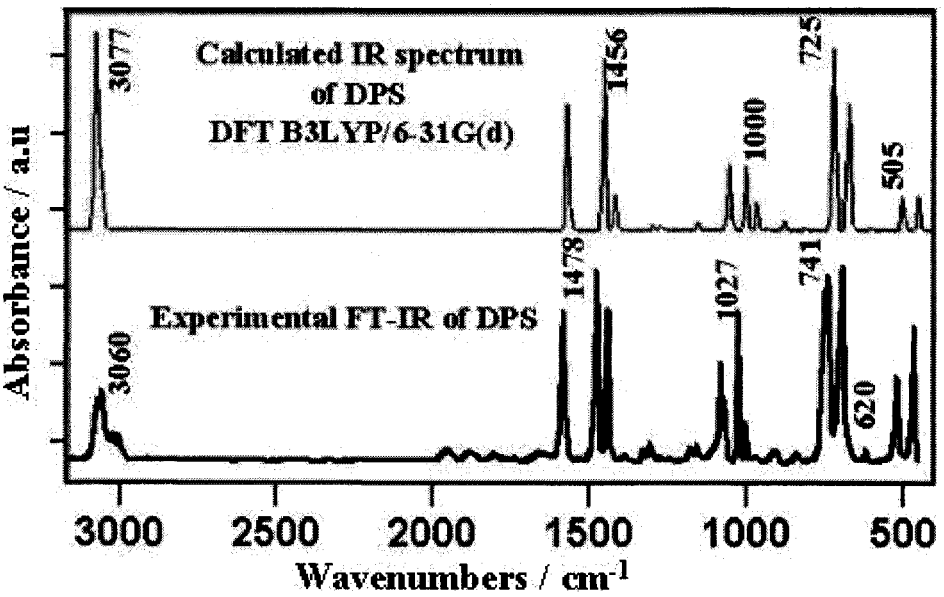

Figure 28: Calculated IR and experimental FT-IR spectra of DPS.

3.2.1 Diphenyl sulfide SERS on silver and gold colloids

A complete interpretation for the assignment of vibrational fundamentals was given in Table 4. Figure 29, which presents the SERS spectra recorded with the 514 nm laser lines for 50 μl of 10^{-3} M DPS added to silver and gold colloids one at the time, and then casted on glass slide to dry out. Two weak bands can be noticed in the frequency ranged from 2540 cm^{-1} to 2596 cm^{-1} in the SERS spectra obtained from cast silver colloids, which may correspond to S-H stretching vibrations. However, the latter was not observed on gold cast colloids. The bands were also noticed when the liquid (neat) DPS was excited with 514 nm, as well as on SERS using 633 nm and 780 nm lines. The S-H appearance could be explained if DPS undergoes spontaneous photo dissociation and cleavage of C-S bond under exposure to laser irradiation, in absence of metal surface, and that depends on the intensities of the excitation lines. Most publications assign the band 2550 cm^{-1} to S-H stretching mode.[38,70,98] These bands also exist in the spectra taken on silver colloidal solution using 514 nm laser line, as shown in Figure 29. In addition, the features observed in the SERS spectrum at 415,#688,#999,#1024,#1072 and 1578 cm^{-1}, when 514.5 nm was used, are characteristic of the benzenethio group.[36] However, the Ag-S stretching vibration was not observed in the DPS SERS spectra. For comparison, the SERS spectra of DPS on Au colloid were also recorded and from these results it was extracted that the DPS adsorbed without cleavage of the C-S bond using 514.5 nm line, in contrast with its cleavage on silver colloid. The alignment of the molecule on colloidal gold or silver surfaces might be the reason of the appearance and disappearance of the band at 615 cm^{-1} in the SERS spectra (Figure 29).

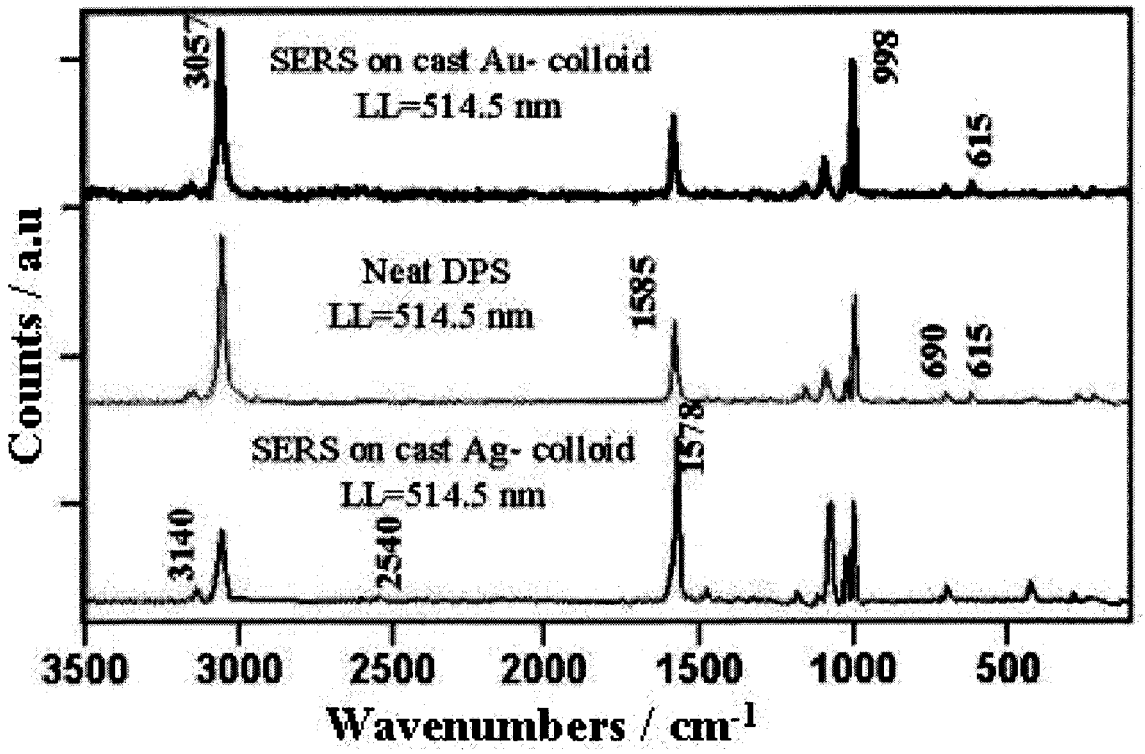

Figure 29: SERS spectra of DPS from the cast gold and silver colloids.

Table 4 The vibrational assignments of DPS and the comparison of SERS on silver colloids with different lines of excitations.

Calculated Frequency (cm^{-1})	Raman Intensity	Observed Raman (cm^{-1})	Cast Ag-sol 633 nm	SERS Ag-sol 514 nm	SERS Ag-sol 633 nm	SERS Ag-sol 780 nm	Assignments
3088	72						C-H str.
3088	419	3058	3052	3057	3053		C-H str.
3083	91						C-H str.
3083	85						C-H str.
3076	92						C-H str.
3076	59						C-H str.
3065	72						C-H str.
3065	190						C-H str.
3058	27						C-H str.
3057	39						C-H str.
		2596	2589	2596			S-H str
		2539	2535	2540			S-H str
1579	100	1580	1570	1578		1569	C-C str.
1576	50						C-C str.
1570	10						C-C str.
1565	5.0	1479	1470	1476	1470	1471	C-C str.

Calculated Frequency (cm^{-1})	Raman Intensity	Observed Raman (cm^{-1})	Cast Ag-sol 633 nm	SERS Ag-sol 514 nm	SERS Ag-sol 633 nm	SERS Ag-sol 780 nm	Assignments
1462	4.0						Ring str.
1460	0.0						Ring str.
1427	3.0	1438	1431	1432	1432	1432	Ring str.
1421	1.0			1374	1387	1388	Ring str.
1304	6.0	1327		1330			Ring str.
1303	2.0		1293		1292	1293	Ring str.
1282	1.0	1271	1274				Ring str.
1269	0.0						Ring breath
1161	6.0	1176		1184	1178	1183	C-H bend.
1160	4.0	1155	1135		1136	1138	C-H bend.
1141	3.0						C-H bend.
1141	10.0		1107	1106	1107	1106	C-H bend.
1070	66	1092	1069	1072	1068	1070	C-H bend.
1063	0.0						C-H bend.
1061	0.0						C-H bend.
1058	10						C-H bend.
1009	50	1025	1019	1024	1019	1020	Ring str.
1008	8.5						Ring breath
974	68	998	995	999	995	997	Ring breath
973	7.0						Ring breath
959	0.0						C-H bend.
959	0.0						C-H bend.
936	0.0						C-H wag.
936	0.0						C-H wag.
887	0.0						C-H wag.
885	0.0						C-H wag.
822	7.0	837	831				C-H wag.
820	3.0						C-H wag.
734	4.0	740	834				C-H wag.
725	0.0						C-H wag.
683	4.0	695	688	693	688	689	C-C-C bend. + C-S str.
682	0.0						C-C-C bend. + C-S str.
677	0.0						Ring def.
673	0.0						Ring def.
605	8.0	615	612		611		C-S str.
605	0.0						C-C-C bend. + C-S str.
506	1.5	513	539				Ring def.
456	0.2	467	466		465	467	Ring def.
425	0.0						Ring def.

Calculated Frequency (cm^{-1})	Raman Intensity	Observed Raman (cm^{-1})	Cast Ag-sol 633 nm	SERS Ag-sol 514 nm	SERS Ag-sol 633 nm	SERS Ag-sol 780 nm	Assignments
402	1.2	411	415	415	415	415	Ring def.+ C-S bend
397	0.0						Ring def.
395	0.0						Ring def.
266	0.0						Skelal. def.
262	4.0	268	285	280			Skelal. def.
195	7.0	215		236			Skelal. def.
169	1.3	186	176		179	180	Ring wag.
62	10					162	Ring wag.
32	15					138	Ring wag.
21	0.0						Ring wag.

3.2.2 Surface enhanced Raman scattering of DPS on silver islands

The SERS work on DPS parallels to that carried out for DPDS. DPS 10^{-3} M in methanol was cast on 6 nm silver film and SERS spectra were collected using different laser lines as described in the case of DPDS. For the sake of comparison, different SERS spectra of DPDS and DPS were put together in Figure 30. As it was mentioned, the SERS bands of DPS were assigned with the help of a DFT computation (B3LYP at 6-31G (d)) level of theory, and SERS spectra were obtained with three laser lines on silver colloids and silver films. The minimized geometry of DPS is again shown as an inset in Figure 30. The most relevant information derived from this work, is that the C-S stretching vibrations are calculated to be below 700 cm^{-1}. There are two calculated modes (at 669 cm^{-1} and 670 cm^{-1}), which according to atomic displacements and relative intensities, may be assigned to C-S stretching vibrations. Experimentally, the spectrum of DPS has a band at 615 cm^{-1}, which is clearly detected in the spectrum of the neat material, as shown in the top spectrum of Figure 30. The latter band is not found in the SERS spectra of DPS obtained on silver colloids, or on silver films, with 514.5 or 633 nm excitation, as can be seen in Figure 30. The SERS spectrum of DPDS taken under similar condition has been

included in the same figure to highlight the fact that the obtained SERS spectrum corresponds to the same adsorbed species, independent of whether the starting material was the DPDS or the DPS molecule. Kim's group[99] has reported the cleavage of the C-S bond in benzyl phenyl sulfide, producing mainly the phenyl sulfide complex on the silver surface, due to photodecomposition. Here, we found that the cleavage readily takes place on silver colloids, and that the same spectrum is obtained for SERS in silver colloids solutions (last spectrum in Figure 30) as it is obtained from aggregated colloids that are cast onto glass surfaces (second last spectrum in the Figure marked as Ag colloids). For silver films, our results are in full agreement with previous findings.[36] Finally, as can be seen in Figure 30, the Ag-S stretching vibration is not seen with enough relative intensity to be clearly identified in any of the SERS spectra except in the case of salt complex of DPDS.

Table 5 The SERS spectra of DPS cast on the silver films and from silver and gold colloids.

Observed Raman (cm^{-1})	Cast Au-sol. 514 nm	Cast Ag-sol. 780 nm	Cast on Ag-film 514 nm	Cast on Ag-film 633 nm	Cast on Ag-film 780 nm
3146	3150		3140	3140	
3058	3057	3053	3056	3057	3053
2596		2570			
2539		2520			
1580	1581	1570	1575	1568	1569
1479		1467	1470	1470	1469
1438	1439	1430		1430	1430
1327		1386			
1271		1297		1290	
1176		1184	1171	1178	1183
1155	1155	1136	1151	1156	1158
1092	1092	1070	1072	1069	1070
1025	1024	1019	1018	1019	1019

Observed Raman (cm^{-1})	Cast Au-sol. 514 nm	Cast Ag-sol. 780 nm	Cast on Ag-film 514 nm	Cast on Ag-film 633 nm	Cast on Ag-film 780 nm
998	999	994	996	997	996
837		820			820
740	739	734		740	736
695	696	689	688	686	688
615	615	613	611		614
467	474	484	474	462	464
411	409	415	413	415	415
	302				308
268	270	260			254
215	213	203		192	
186	180	179		178	178
		157			158
		137			137
		112			114

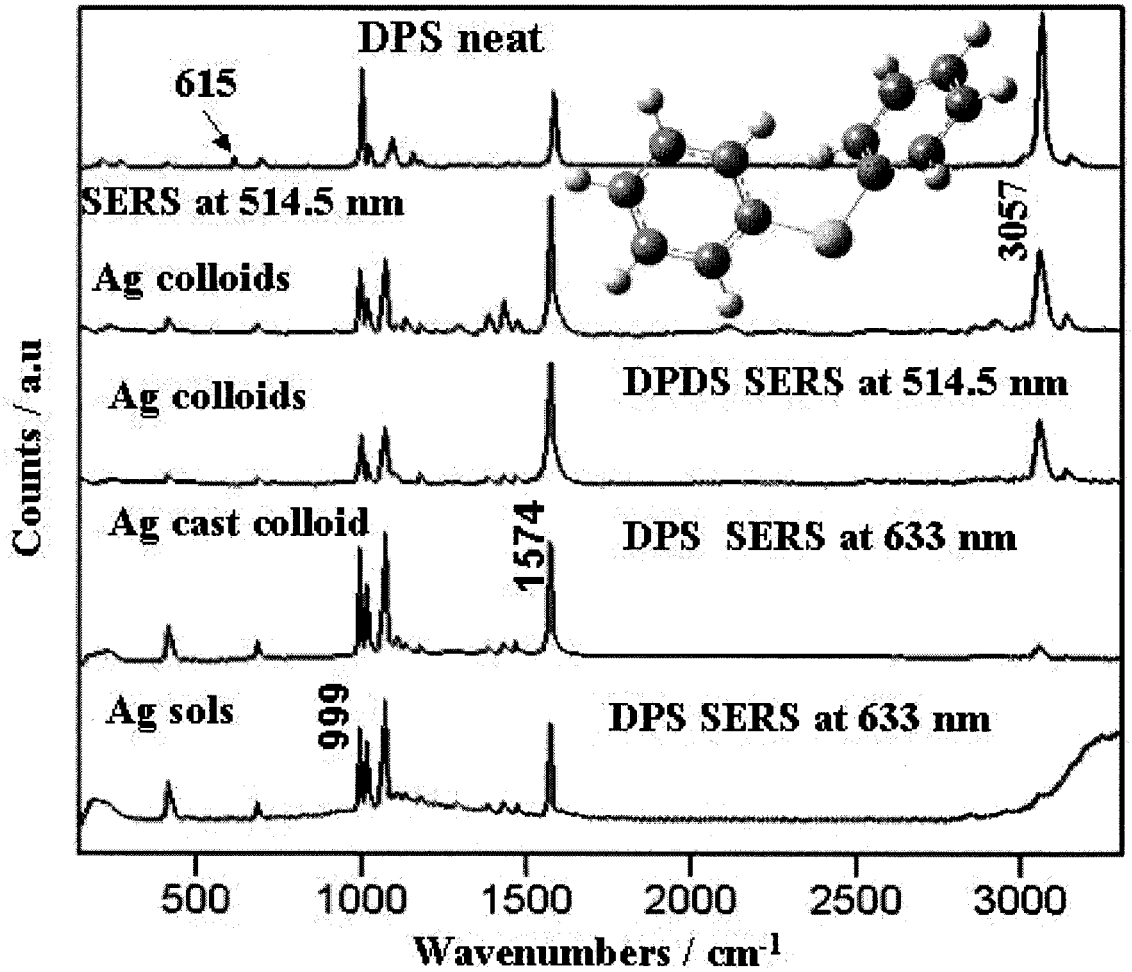

Figure 30: The comparison between SERS spectra of DPS and DPDS on silver colloids.

4.0 SINGLE MOLECULE DETECTION OF A PERYLENE DERIVATIVE

The molecule *n*Bu-PTCDA-$(CH_2)_4$-NH_2 has been chosen as the target molecule for studies involving SMD. Therefore, a basic characterization including the electronic and vibrational spectra of this molecule is required.

4.1 Electronic absorption

Figure 31 shows the UV-vis absorption spectrum of the *n*Bu-PTCDA-$(CH_2)_4$-NH_2 diluted in dichloromethane and in Figure 32 its molecular structure.

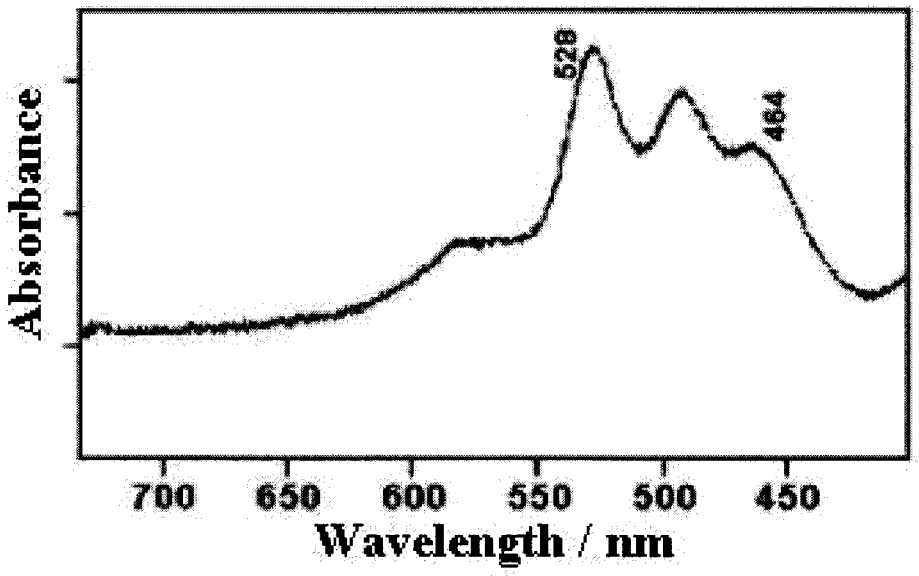

Figure 31: The electronic spectrum of *n*Bu-PTCDA-$(CH_2)_4$-NH_2, 10^{-3} M in CH_2Cl_2.

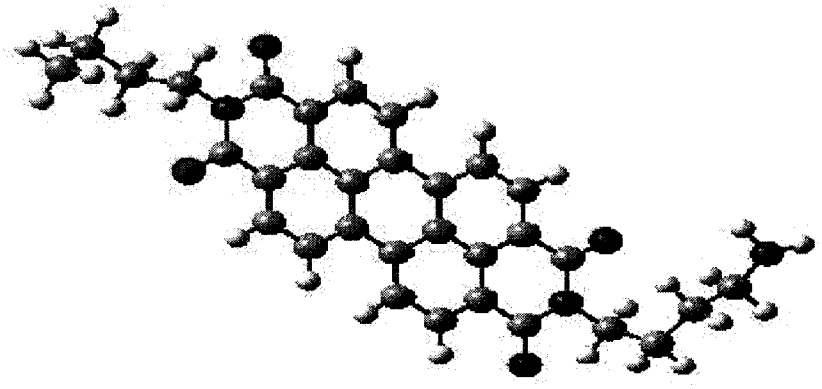

Figure 32: The optimized geometry of *n*Bu-PTCDA-$(CH_2)_4$-NH_2.

The absorption spectra of the perylene tetracarboxylic derivatives have been calculated and assigned previously.[100] The observed visible absorption spectrum consists of a one electronic transition with the corresponding vibronic structure associated with $\pi \rightarrow \pi^*$ transition of the perylene moiety from the ground electronic state to any of the vibrational states within the higher electronic state. The transitions 0-0 at 528 nm, 0-1 at 493 nm, and 0-2 at 464 nm can be seen. The optimized molecular geometry given in Figure 32 is the result of a theoretical calculation using the DFT B3LYP/6-31G(d) level of theory, and was selected from two different levels of calculations, which were carried out.

4.2 Molecular vibrations: infrared and Raman spectra

The molecular structure of the *n*Bu-PTCDA-$(CH_2)_4$-NH_2 shown in Figure 32 indicates that the molecule belongs to the C_1 symmetry group and all vibrational fundamentals are Raman and infrared active. There are 192 vibrational modes resultant from 3N-6 degrees of freedom, as the molecule possesses 66 atoms. The in-plane and out-of-plane vibrational modes are dominated by the planar chromophore in the

molecule. All vibrational assignments were helped using *ab initio* theoretical computations of frequencies and intensities. In fact, two calculations were carried out with different levels of theory; DFT B3LYP/6-31G basis set and HF/2-31G basis set. DFT has shown a better agreement with the experimental spectra. The calculated and experimental Raman spectra as well as the calculated and experimental FT-IR spectra are in good agreement as can be seen in Figures 33 and 34 respectively. The scaling factor used at this level was 0.9614 and Gaussian98[85] software for windows was used for the calculation. The calculated and observed wavenumbers in the Raman spectra of *n*Bu-PTCDA-$(CH_2)_4$-NH_2 and the normalized intensities are listed in Table 6. One of the lateral groups of *n*Bu-PTCDA-$(CH_2)_4$-NH_2 terminals has a $-CH_2$-CH_2-CH_2-CH_2-NH_2 directly attached to the perylene core, which increases the ability of a chemisorption process when the molecule adsorbs on active surface substrates. In addition, this terminal group is considered to be one of the factors for the colloidal silver particles starting to aggregate immediately. The color change of the solution is the physical evidence of the chemical adsorption. Concentrations as low as 10^{-9} to 10^{-12} M can be detected either using cast films or colloidal solutions. At such concentrations, it was assumed that no more than one molecule would be attached to a single silver cluster.[101,102]

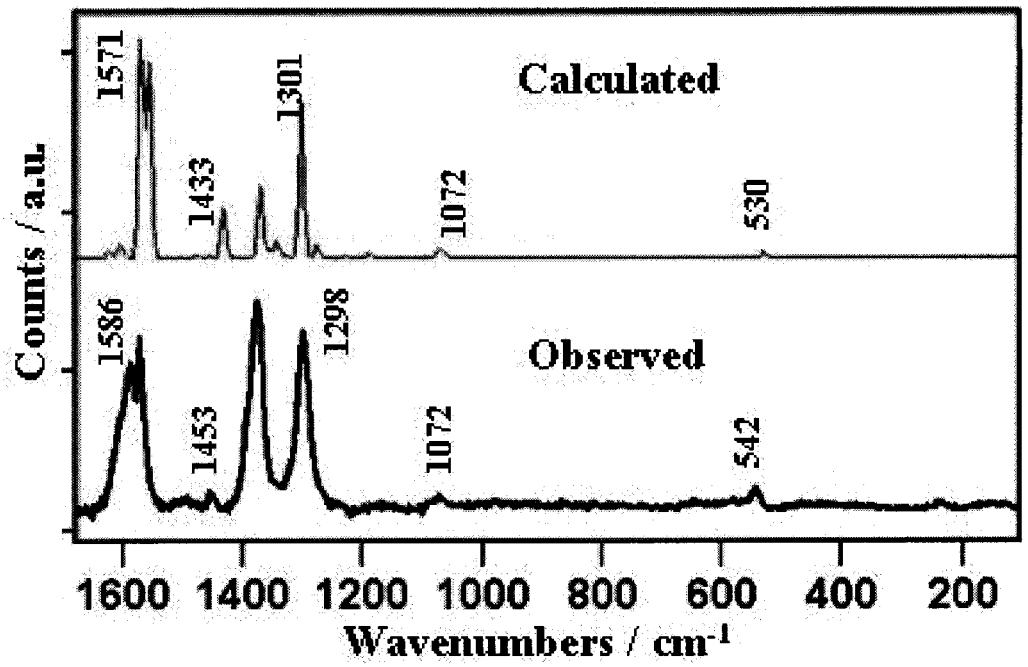

Figure 33: The calculated and experimental Raman spectra of *n*Bu-PTCDA-$(CH_2)_4$-NH_2.

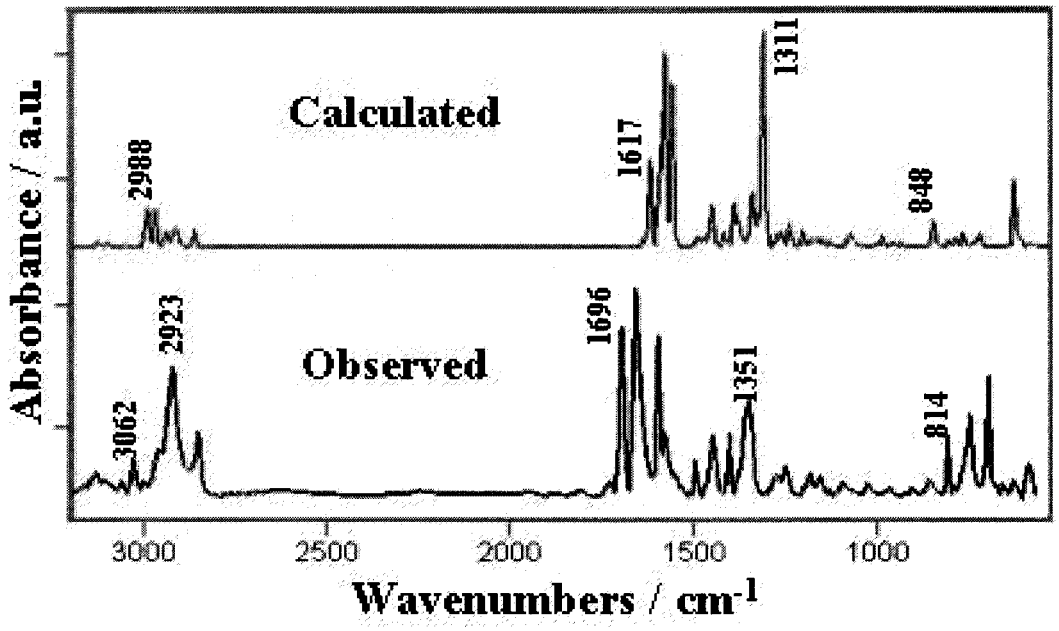

Figure 34: The calculated and experimental FT-IR spectra of *n*Bu-PTCDA-$(CH_2)_4$-NH_2.

4.3 Single molecule detection on silver and gold colloids

The existence of two different contributors, CT and EM, to the Raman signals in SERS or SERRS, and the advantage of the more sensitive detectors in the new Raman instruments have made the detection of a single molecule possible using Raman technique. The resonance Raman effect and surface-enhancement are the major effects that increase Raman cross-sections to a detectable level.[101] In this work, two different substrates were used in two different forms: the first was the addition of the analyte (*n*Bu-PTCDA-$(CH_2)_4$-NH_2) to a silver colloidal solution where they were probed in solution using a 40x immersion lens. The second was to use Raman measurements for the cast gold-analyte complex on a glass slide. The insolubility of perylene derivatives in water is well-known. Thus, stock 10^{-3} M solution of the analyte was prepared using 10% trifluoroacetic acid (TFA) and 90% dichloromethane spectroscopic grade solvents. TFA is necessary since *n*Bu-PTCDA-$(CH_2)_4$-NH_2 is not soluble in conventional organic solvents either. Diluted solutions ranging from 10^{-5}-10^{-12} M were prepared by serial dilutions using dichloromethane. Both colloidal substrates silver and gold were prepared using sodium citrate as a reducing agent following the method described in Chapter II. The maximum of the UV-vis absorption bands was at 408 nm and 527 nm for silver and gold, respectively, as shown in Figures 4 and 6. In the first case, using silver colloids, the measurements of SERRS was achieved by transferring a concentrated solution of *n*Bu-PTCDA-$(CH_2)_4$-NH_2, ranging from 10^{-3}-10^{-12} M, to the colloids. Volumes from 10 μL to 50 μL of the analyte solutions were dropped in 3 mL of silver colloids, the mixture shacked for three minutes. It is worth mentioning that neither colloidal stabilizers, nor an active agent, were added before or during the SERRS measurements. Because of the

decrease in concentration from nanoliter to picoliter, higher accumulations of scans ranging from 80 to 100 were implemented to get smoother spectra. During the measurements, 50 μL of *n*Bu-PTCDA-$(CH_2)_4$-NH_2 solution, with concentrations ranging 10^{-9}-10^{-12} M, were mixed with 3 mL of silver colloids one at the time. A color change of the complex was an indication of direct chemical adsorption of the PTCD molecule through its –CH_2-CH_2-CH_2-CH_2-NH_2 group. The number of molecules in 10^{-12} M solution was calculated to be 10036 molecules/μL. Assuming that the scattering volume of the immersion lens is a picoliter, it was found that the total number of molecules in that scattering volume is about 0.01 molecules on average. It is known that at this low analyte concentration, the chance of the molecular aggregation is unlikely.[10] The Figure 35 shows clear SERRS signals of ca. 0.01 molecules at 10^{-12} M of the analyte, reaching the SM level. The calculated, the observed wavenumbers, and relative intensities are listed in Table 6.

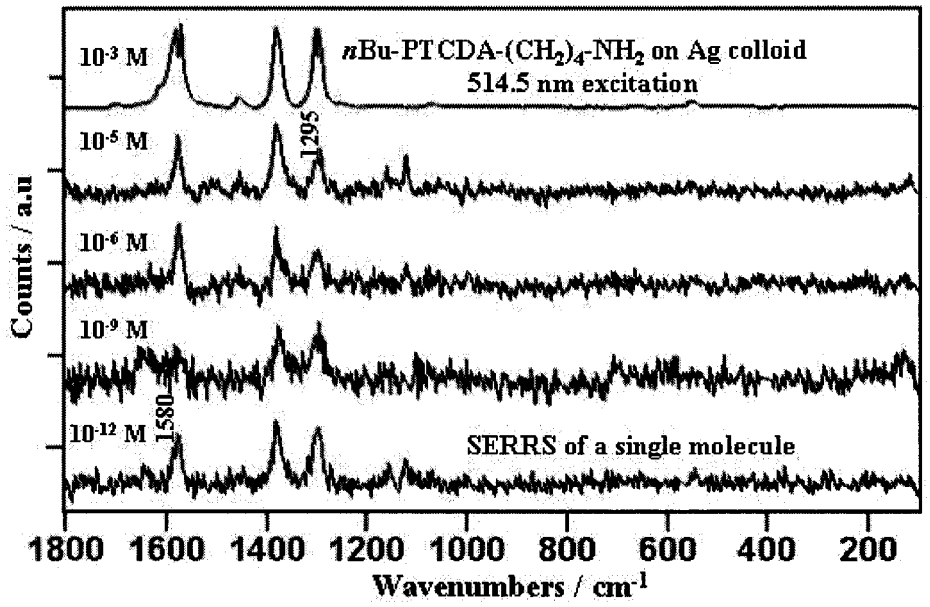

Figure 35: SERRS of *n*Bu-PTCDA-$(CH_2)_4$-NH_2 on Ag colloids.

The second set of experiments was carried out using gold colloid-analyte complexes cast on glass slides. The reaction of the *n*Bu-PTCDA-$(CH_2)_4$-NH_2 with gold nanoparticles were apparent as the color changed from light pink to dark pink. SERRS measurements were not different from the work done on silver colloids except for the use of micro Raman with a 50x objective. A 514.5 nm laser line was used for excitation. 40 μL of the analyte (as low as 10^{-9} M in concentration) was added to 3 mL of gold colloids, the mixture shacked for three minutes, and left for half an hour for the reaction to be completed, 20 μL of this complex was then cast on the glass slide and left to dry in isolated dark container. The scattering area of the 50x lens is ca. 1 μm^2 and it is important to know the number of molecules in this scattering area. Using a simple calculation it was found that the number of moles 40 x 10^{-6} L x 10^{-9} moles/L = 4 x 10^{-14} moles. Dividing by 3000 μL of Au-colloidal solution it gives the number of moles per 1 μL and that is equal to 1.3 x 10^{-17} moles/μL. The numbers of molecules per 20 μL drop left to dry on 1 cm^2 area was about 1.6 molecule/μm^2. The SERRS spectra of a single molecule on cast gold colloids are shown in Figure 36.

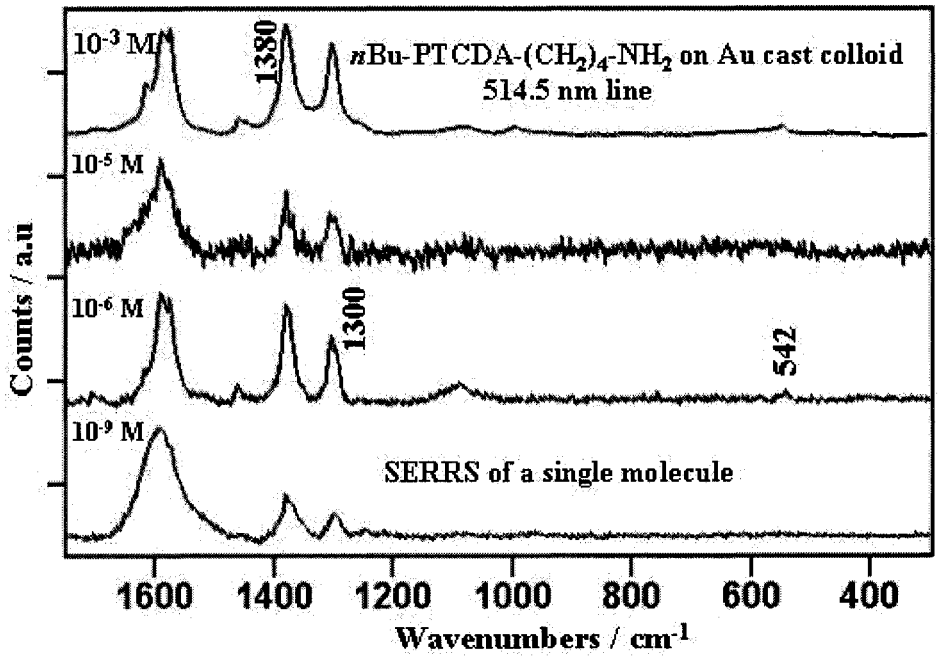

Figure 36: SERRS spectra of *n*Bu-PTCDA-$(CH_2)_4$-NH_2 on gold cast colloids.

Table 6 The assignment of vibrational fundamentals of observed RRS/SERRS of *n*Bu-PTCDA-$(CH_2)_4$-NH_2 on silver colloids and gold cast colloids. Scaling factor is 0.9614.[85]

Calculated Frequency (cm^{-1})	Normalized Raman Intensity	Observed Resonance Raman (RRS) 514.5 nm	SERRS on Ag colloids 514.5 nm	SERRS on Au cast colloid 514.5 nm	Assignment
3496	0				C-H str.
3386	0				C-H str.
3128	0				C-H str.
3128	0				C-H str.
3119	0				C-H str.
3119	0				C-H str.
3110	0				C-H str.
3110	0				C-H str.
3102	0				C-H str.
3101	0				C-H str.
3057	0				C-H str.
3054	0				C-H str.
2999	0				C-H str.
2995	0				C-H str.
2993	0				C-H str.

Calculated Frequency (cm^{-1})	Normalized Raman Intensity	Observed Resonance Raman (RRS) 514.5 nm	SERRS on Ag colloids 514.5 nm	SERRS on Au cast colloid 514.5 nm	Assignment
2991	0				C-H str.
2977	0				CH_2-sym. str.
2974	0				CH_2-sym. str.
2973	0				CH_2-sym. str.
2949	0				CH_2-sym. str.
2940	0				CH_2-sym. str.
2926	0				CH_2-antisym. str.
2925	0				CH_2-antisym. str.
2912	0				CH_2-antisym. str.
2919	0				CH_2-antisym. str.
2911	0				CH_2-antisym. str.
2868	0				CH_2-antisym. str.
1642	0				C=O str.
1626	3	1610	1614	1611	C=O str.
1624	0				C=O str.
1607	7	1588	1580	1584	C=O, C=C str.
1597	0				C=C str.
1584	0				C=C str.
1572	100	1571	1571	1572	C=C str.
1571	0				OCN bend.
1565	0				Ring str.+ C-H bend
1563	0				Ring str. + C-H bend
1559	0				Ring str. + C-H bend
1516	0				Ring str. + C-H bend.
1504	0				Ring str. + C-H bend.
1498	0				CH_2 bend.

Calculated Frequency (cm^{-1})	Normalized Raman Intensity	Observed Resonance Raman (RRS) 514.5 nm	SERRS on Ag colloids 514.5 nm	SERRS on Au cast colloid 514.5 nm	Assignment
1493	0				Antisym. CH_3 str.
1489	0				Antisym. CH_3 str.
1480	0				CH_2 bend.
1480	0				CH_2 bend.
1478	0				CH_2 bend.
1478	0				CH_2 bend.
1470	0				C-H bend.
1460	0				C-H bend.
1457	0				CH_2 bend.
1455	0				CH_2 bend.
1435	25	1454	1456	1457	Perylene ring str.
1422	0				Ring str. + C-H bend
1408	0				CH_2 bend.
1396	0				CH_2 bend.
1395	0				Ring str. + C-H bend.
1390	0				Ring str. + CH_2 bend.
1383	0				Butyl CH_2 bend.
1374	35	1378	1380	1377	Perylene ring str.
1371	0				Butyl CH_2 bend.
1360	0				Butyl CH_2 bend.
1354	0				CH_2 bend.
1346	0				Ring str.+ C-H bend.
1345	0				Ring str.+ C-H bend.
1344	0				Ring str.+ C-H bend.
1338	0				CH_2 bend.
1332	0				CH_2 bend.
1329	0				Ring str. + CH_2 bend.

Calculated Frequency (cm^{-1})	Normalized Raman Intensity	Observed Resonance Raman (RRS) 514.5 nm	SERRS on Ag colloids 514.5 nm	SERRS on Au cast colloid 514.5 nm	Assignment
1316	0				Ring str. + CH_2 bend.
1313	0				NH_2, CH_2 bend.
1311	0				Ring str.+ C-H bend.
1305	74	1300	1300	1301	Perylene ring str.
1291	0				C-H bend.
1281	0				C-H bend.
1279	6	1295	1295sh	1294sh	Ring str. + CH_2 bend.
1268	0				CH_2 bend.
1265	0				C-H bend. in plane.
1257	0				C-H bend in plane.
1244	0				C-H bend in plane.
1231	0				C-H bend in plane.
1209	0				C-H bend in plane.
1199	0				C-H bend in plane.
1194	0				C-H bend in plane.
1192	0				C-H bend in plane.
1185	0				C-H bend in plane.
1173	0				Ring str. + CH_2 bend.
1158	0				CH_2 bend.
1137	0				C-H bend. in plane.
1136	0				C-H bend in plane.
1128	0				C-H bend in plane.

Calculated Frequency (cm^{-1})	Normalized Raman Intensity	Observed Resonance Raman (RRS) 514.5 nm	SERRS on Ag colloids 514.5 nm	SERRS on Au cast colloid 514.5 nm	Assignment
1113	0				C-H bend in plane.
1087	0				C-H bend in plane.
1078	0				C-H bend in plane.
1075	4	1072	1065	1079	C-H bend in plane.
1066	0				NH_2 bend.
1050	0				Butyl CH_2 bend.
1048	0				NH_2 bend.
1036	0				Ring def.
1009	0				Ring def.+ NH_2 bend.
992	0				C-H bend. in plane.
992	0				C-H bend. in plane.
989	0				C-H bend. in plane.
985	0				C-H bend. in plane.
981	0				C-H bend. in plane.
969	0				CH_2 bend.
962	0				CH_2 bend.
944	0				CH_2 bend.
935	0				CH_2 bend.
912	0				CH_2 bend.
898	0				Ring def.
869	0				C-H wag.
857	0				C-H wag.
856	0				C-H wag.
855	0				C-H wag.
855	0				C-H wag.
854	0				C-H wag.
847	0				C-H wag.
817	0				C-H wag.
811	0				C-H wag.
795	0				C-H wag.

Calculated Frequency (cm^{-1})	Normalized Raman Intensity	Observed Resonance Raman (RRS) 514.5 nm	SERRS on Ag colloids 514.5 nm	SERRS on Au cast colloid 514.5 nm	Assignment
794	0				C-H wag.
790	0				C-H wag.
775	0				C-H wag.
769	0				C-H wag.
749	0				C-H wag.
741	0				C-H wag.
738	0				C-H wag.
735	0				C-H wag.
729	0				C-H wag.
728	0				C-H wag.
707	0				C-H wag.
699	0				C-H wag.
693	0				Ring def.
661	0				Ring def.
650	0				Ring def.
635	0				Ring def.
620	0				Ring def.
617	0				Ring def.
609	0				Ring def.
594	0				Ring def.
578	0				Ring def.
569	0				Ring def.
533	3	542	549	546	Ring def.
524	0				Ring def.
511	0				Ring def.
499	0				Ring def.
480	0				Ring def.
474	0				Ring def.
468	0				Ring def.
462	0				Ring def.
444	0				Ring def.
440	0				Ring bend.
435	0				Ring bend.
425	0				Ring str.+ CH_2 bend.
397	0				Ring def.+ C-H bend.
387	0.1		391	390	Ring str.+ CH_2 bend.
385	0				Ring str.+ CH_2 bend.

Calculated Frequency (cm^{-1})	Normalized Raman Intensity	Observed Resonance Raman (RRS) 514.5 nm	SERRS on Ag colloids 514.5 nm	SERRS on Au cast colloid 514.5 nm	Assignment
382	0				CH_2 twist
380	0				Ring def.
365	0				Ring def.
359	0				Ring bend.
338	0				Ring bend.
321	0				Ring bend.
312	0				Ring def.+ C-H bend.
295	0				Ring def.+ C-H bend.
273	0				CH_3 bend.
271	0				CH_3 bend.
269	0				Ring bend.
234	0				Ring bend. + CH_3 twist
227	0				CH_3 bend.
211	0				NH_2 twist
203	0				NH_2 twist
183	0				Ring bend.
181	0				Butyl CH_3 torsion
170	0				Ring def.
148	0				Ring bend.
142	0				Butyl CH_2 twist
138	0				Butyl group str.
113	0				Butyl NH_2 torsion
106	0				CH_2 torsion
101	0				CH_2 torsion
91	0				Ring def.
81	0				Ring def.+ CH_2 bend.
71	0				Ring bend.
65	0				Ring def.
45	0				Butyl CH_3 torsion
39	0				Ring def.
34	0				Ring def.+ NH_2 twist

Calculated Frequency (cm^{-1})	Normalized Raman Intensity	Observed Resonance Raman (RRS) 514.5 nm	SERRS on Ag colloids 514.5 nm	SERRS on Au cast colloid 514.5 nm	Assignments
28	0				Ring def.
22	0				Ring def.
19	0				Ring def.
12	0				Ring def.

4.4 Resonance Raman spectra of single molecules: overtones and combinations

The SERRS spectrum of *n*Bu-PTCDA-$(CH_2)_4$-NH_2 contains a small number of characteristic fundamentals that can be attributed to the perylene chromophore moiety. Characteristic vibrational modes of the perylene moiety are observed in resonance Raman spectra at 1293, #1375, #1571 and 1580 cm^{-1}. The C=O stretching is also observed at 1610 cm^{-1}. The lower wavenumber band is prominent in RRS of the bulk at 1378 cm^{-1}, while the higher wavenumber band at 1580 cm^{-1} is prominent in SERRS. Consequently, the SERRS does not depend necessarily on RRS and is not to be considered as an amplification of resonance Raman spectrum. Table 7 contains the fundamentals, combinations and overtones characteristics of the PTCDA derivative and their assignments. Both (RRS and SERRS) spectra are mainly due to the perylene tetracarboxylic acid moiety, and the difference between them is identified as relative SERRS intensity changes when compared with the same normal modes present in the RRS spectra. The anharmonicity of the molecular vibrations of this molecule seems to be large in general, and consequently the overtones and combination bands can be observed. RRS and SERRS spectra of *n*Bu-PTCDA-$(CH_2)_4$-NH_2 show fundamentals, combinations and overtones characteristic of three fundamental stretching ring vibrations of the perylene tetracarboxylic chromophore.[102] Figure 37 shows both RRS and SERRS spectra of *n*Bu-PTCDA-$(CH_2)_4$-NH_2. Although the excitation line in this particular investigation

was only 514.5 nm, the change of the relative intensities of the overtone bands with respect to other excitation line was recently investigated.[103] The second overtone progression bands were also observed, assigned and marked. However, that was not the case in the lowest concentration of the analyte, where only the first overtones and combination bands were seen on the gold cast colloid with concentration of 10^{-9} M of the *n*Bu-PTCDA-$(CH_2)_4$-NH_2. It might be evidence of overtones, and combination of a single molecule adsorbed on Au aggregated colloids. A very recent study within our group on three of the PTCD derivatives stated that the single molecule SERRS allows the observation of overtones and combinations using UV Raman excitation.[104] Finally, there are few large molecules for which the overtones and combination of skeletal vibrations are clearly observed in the condensed phase.[105]

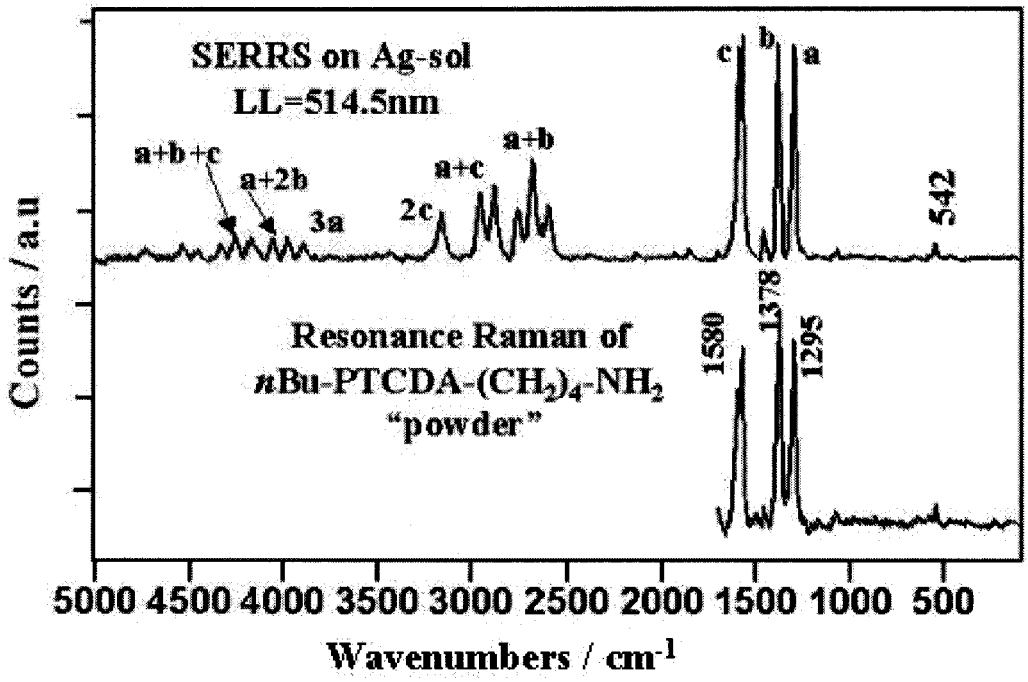

Figure 37: The RRS, SERRS, overtones and combinations of *n*Bu-PTCDA-$(CH_2)_4$-NH_2.

Table 7 Overtones and combinations bands observed in the SERRS of *n*Bu-PTCDA-$(CH_2)_4$-NH_2 chemisorbed on silver colloid.

Observed fundamentals 514.5 nm	Symbols	Calculated overtones and combinations	Assignments
1295	a		Ring str. +C-H bending.
1300			Perylene ring str.
1378	b		Perylene ring str.
1453			Perylene ring str.
1571			Perylene ring str.
1580	c		Perylene ring str.
Observed first overtones			
2597	2a	2590	
2676	a+b	2673	
2755	2b	2756	
2877	a+c	2875	
2954	b+c	2958	
3158	2c	3160	
Observed second overtones			
3892	3a	3885	
3973	2a+b	3968	
4053	a+2b	4051	
4168	2a+c	4170	
4253	a+b+c	4253	
4329	2b+c	4336	

4.5 Molecular orientation

PTCD is one of the organic dye molecules that can be used in electroluminescent devices. These devices are made mainly using thin organic film. The molecular orientation in the organic film plays an important role in the electrical and optical properties of the device. The molecular orientation in a film can be determined qualitatively using the surface selection rules[26], which can be shortly described as follow: in the case of transmission mode, the polarization of a normal incident radiation lies on the substrate plane (parallel to the surface). On the other hand, in the case of reflection

mode (RAIRS), the reflecting surface polarizes the light perpendicularly to the substrate plane. Therefore, the vibrational modes related to the induced dipole moment parallel to the substrate will dominate the spectrum in the transmission mode while those related to the induced dipole moment perpendicular to the substrate will dominate the RAIRS spectrum. A KBr pellet can act as a reference of a random molecular organization.

Figure 38 presents the transmission spectrum for *n*Bu-PTCDA-$(CH_2)_4$-NH_2 dispersed in a KBr pellet at the bottom of the figure, and the RAIRS spectrum on smooth silver mirror at the top. The change of the observed relative intensity in the transmission spectrum of the molecule dispersed in a KBr pellet is obvious comparing to the RAIRS spectrum obtained from the 30 nm evaporated organic film on silver mirror, by following the key bands (C-H wag. at ca. 708 cm^{-1}, C=O symmetric stretching at 1696 cm^{-1} and C=O anti-symmetric stretching 1658 cm^{-1}) shows that the molecule is organized head-on (normal) the surface mainly. It must be considered that C-H wagging is perpendicular to the PTCD core, the C=O symmetric stretching is in the plane of PTCD core and parallel to edge of the core while the C=O anti-symmetric stretching is in the plane of PTCD core and parallel to head of the core. The orientation analysis was based on observing the change in the relative intensity of C-H wagging as first step. The band at 700 cm^{-1} wavenumber in transmission spectrum was hardly seen in the RAIRS spectra, and raises the possibility of head-on or edge-on adsorption. The intensities changes at higher wavenumbers where C=O anti-symmetric vibrations were observed, the symmetric C=O stretching at 1696 cm^{-1} became more intense in RAIRS. It was concluded that the molecule adsorbs head-on with little tilting. The transmission and RAIRS observed frequencies were listed in the Table 8.

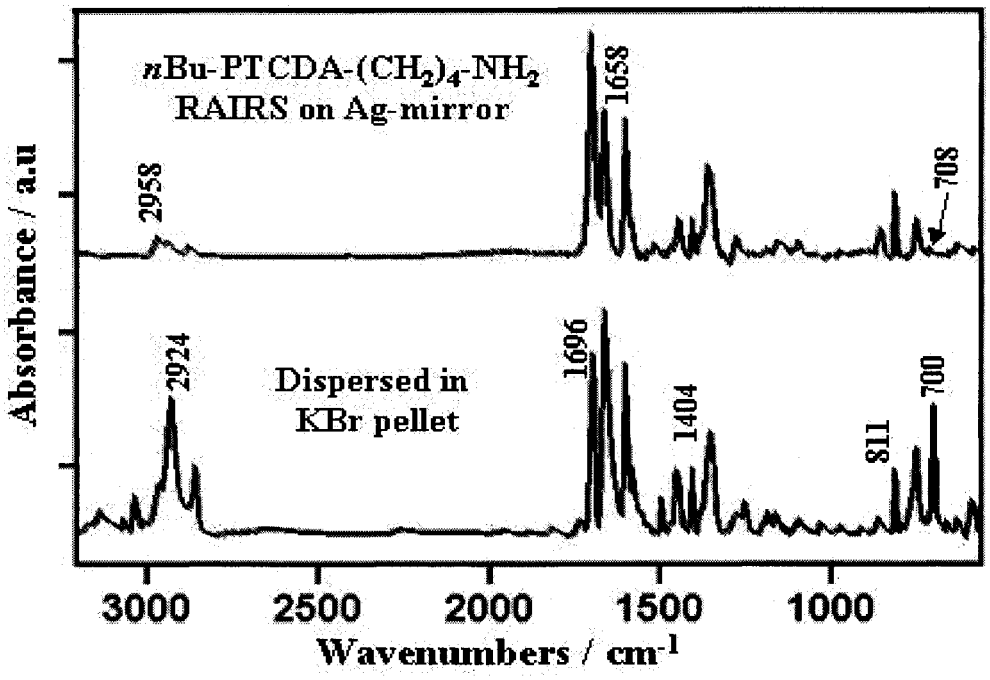

Figure 38: The FT-IR transmission and RAIRS spectra of *n*Bu-PTCDA-$(CH_2)_4$-NH_2.

Table 8 Calculated fundamentals, observed FT-IR transmission and RAIRS bands of *n*Bu-PTCDA-$(CH_2)_4$-NH_2.

Calculated frequency (cm^{-1})	Normalized IR intensity	Transmission (KBr pellet)	RAIRS (silver mirror)	Assignment
3496	0			C-H str.
3386	0			C-H str.
3128	2	3127		C-H str.
3128	0			C-H str.
3119	0			C-H str.
3119	0			C-H str.
3110	0			C-H str.
3110	0			C-H str.
3102	0			C-H str.
3101	0			C-H str.
3057	0			C-H str.
3054	0			C-H str.
2999	7	3063		C-H str.
2995	0			C-H str.
2993	4	3028		C-H str.
2991	0			C-H str.

Calculated frequency (cm^{-1})	Normalized IR intensity	Transmission (KBr pellet)	RAIRS (silver mirror)	Assignment
2977	0			CH_2-sym. str.
2974	0			CH_2-sym. str.
2973	14	2924	2958	CH_2-sym. str.
2949	0			CH_2-sym. str.
2940	0			CH_2-sym. str.
2926	0			CH_2-antisym. str.
2925	0			CH_2-antisym. str.
2919	0			CH_2-antisym. str.
2912	0			CH_2-antisym. str.
2911	0			CH_2-antisym. str.
2868	8	2853	2858	CH_2-antisym. str.
1642	0	1696	1697	C=O str.
1626	0			C=O str.
1624	34	1658	1658	C=O sym. str.
1607	0			C=O str.
1597	46		1595	C=C str.
1584	92	1593		C=C str.
1572	0			C=C str.
1571	0			OCN bend.
1565	0			Ring str.+ C-H bend
1563	45	1577	1579	Ring str. + C-H bend
1559	0			Ring str. + C-H bend
1516	0			Ring str. + C-H bend.
1504	0			Ring str. + C-H bend.
1498	2	1494	1505	CH_2 bend.
1493	0			Antisym. CH_3 str.
1489	0			Antisym. CH_3 str.
1480	0			CH_2 bend.
1480	0			CH_2 bend.
1478	0			CH_2 bend.
1478	0			CH_2 bend.
1470	0			C-H bend.

Calculated frequency (cm^{-1})	Normalized IR intensity	Transmission (KBr pellet)	RAIRS (silver mirror)	Assignment
1460	0			C-H bend.
1457	0			CH_2 bend.
1455	14	1443	1440	CH_2 bend.
1435	0			Perylene ring str.
1422	0			Ring str. + C-H bend
1408	0			CH_2 bend.
1396	0			CH_2 bend.
1395	16	1404	1403	Ring str. + C-H bend.
1390	0			Ring str. + CH_2 bend.
1383	0			Butyl CH_2 bend.
1374	0			Perylene ring str.
1371	0			Butyl CH_2 bend.
1360	0			Butyl CH_2 bend.
1354	0			CH_2 bend.
1346	0			Ring str.+ C-H bend.
1345	0			Ring str.+ C-H bend.
1344	0			Ring str.+ C-H bend.
1338	0			CH_2 bend.
1332	0			CH_2 bend.
1329	0			Ring str. + CH_2 bend.
1316	100	1346	1348	Ring str. + CH_2 bend.
1313	0			Ring str.+ C-H bend.
1311	0			Perylene ring str.
1305	0			C-H bend.
1291	0			C-H bend.
1281	4	1273	1273	Ring str. + CH_2 bend.

Calculated frequency (cm^{-1})	Normalized IR intensity	Transmission (KBr pellet)	RAIRS (silver mirror)	Assignment
1279	0			Ring str. + CH_2 bend.
1268	0			CH_2 bend.
1265	0			C-H bend. in plane.
1257	0			C-H bend in plane.
1244	10	1247	1237	C-H bend in plane.
1231	0			C-H bend in plane.
1209	0			C-H bend in plane.
1199	0			C-H bend in plane.
1194	0			C-H bend in plane.
1192	0			C-H bend in plane.
1185	2	1183	1181	C-H bend in plane.
1173	0			Ring str. + CH_2 bend.
1158	2	1157	1151	CH_2 bend.
1137	0			C-H bend. in plane.
1136	0			C-H bend in plane.
1128	0			C-H bend in plane.
1113	0			C-H bend in plane.
1087	3	1090	1090	C-H bend in plane.
1078	0			C-H bend in plane.
1075	0			C-H bend in plane.
1066	0			C-H bend in plane.
1050	0			C-H bend in plane.
1048	0			NH_2 bend.

Calculated frequency (cm^{-1})	Normalized IR intensity	Transmission (KBr pellet)	RAIRS (silver mirror)	Assignment
1036	0			Ring def.
1009	0			Ring def.+ NH_2 bend.
992	0			C-H bend. in plane.
992	4	1028		C-H bend. in plane.
989	0			C-H bend. in plane.
985	0			C-H bend. in plane.
981	0			C-H bend. in plane.
969	0	968		CH_2 bend.
962	0			CH_2 bend.
944	0			CH_2 bend.
935	0			CH_2 bend.
912	0			CH_2 bend.
898	0			Ring def.
869	0			C-H wag.
857	0			C-H wag.
856	79	855	853	C-H wag.
855	0			C-H wag.
855	0			C-H wag.
854	0			C-H wag.
847	0			C-H wag.
817	0			C-H wag.
811	0			C-H wag.
795	0			C-H wag.
794	2	811	811	C-H wag.
790	0			C-H wag.
775	5	749	746	C-H wag.
769	0			C-H wag.
749	0			C-H wag.
741	0			C-H wag.
738	0			C-H wag.
735	0			C-H wag.
729	5	698	708	C-H wag.
728	0			C-H wag.

Calculated frequency (cm^{-1})	Normalized IR intensity	Transmission (KBr pellet)	RAIRS (silver mirror)	Assignment
707	0			C-H wag.
699	0			C-H wag.
693	0			Ring def.
661	0			Ring def.
650	0			Ring def.
635	32	627		Ring def.
620	0			Ring def.
617	0			Ring def.
609	0			Ring def.
594	0			Ring def.
578	0			Ring def.
569	0			Ring def.
533	0			Ring def.
524	0			Ring def.
511	0			Ring def.
499	0			Ring def.
480	0			Ring def.
474	0			Ring def.
468	0			Ring def.
462	0			Ring def.
444	0			Ring def.
440	0			Ring bend.
435	0			Ring bend.
425	0			Ring str.+ CH_2 bend.
397	0			Ring def.+ C-H bend.
387	0			Ring str.+ CH_2 bend.
385	0			Ring str.+ CH_2 bend.
382	0			CH_2 twist
380	0			Ring def.
365	0			Ring def.
359	0			Ring bend.
338	0			Ring bend.
321	0			Ring bend.

Calculated frequency (cm^{-1})	Normalized IR intensity	Transmission (KBr pellet)	RAIRS (silver mirror)	Assignment
312	0			Ring def.+ C-H bend.
295	0			Ring def.+ C-H bend.
273	0			CH_3 bend.
271	0			CH_3 bend.
269	0			Ring bend.
234	0			Ring bend. + CH_3 twist
227	0			CH_3 bend.
211	0			NH_2 twist
203	0			NH_2 twist
183	0			Ring bend.
181	0			Butyl CH_3 torsion
170	0			Ring def.
148	0			Ring bend.
142	0			Butyl CH_2 twist
138	0			Butyl group str.
113	0			Butyl NH_2 torsion
106	0			CH_2 torsion
101	0			CH_2 torsion
91	0			Ring def.
81	0			Ring def.+ CH_2 bend.
71	0			Ring bend.
65	0			Ring def.
45	0			Butyl CH_3 torsion
39	0			Ring def.
34	0			Ring def.+ NH_2 twist
28	0			Ring def.
22	0			Ring def.
19	0			Ring def.
12	0			Ring def.

CONCLUSION

In this work, colloid preparation and optical properties were deeply investigated. The optical properties of silver colloids prepared by two different reducing agents, citrate and borohydride, were investigated by UV-vis absorption as a function of time (aging). The citrate colloids show shoulders as a sign of aggregation in the UV-vis absorption spectra, as it is preferable to be used in detecting a trace amount of an analyte in liquid. The borohydride colloid shows a better size distribution and less aggregation tendency in suspension. AFM images were taken for organic free aggregates of citrate colloids and with organic (DPDS used for this purpose). The AFM shows that organic additives double the size of the aggregates.

Complete vibrational studies of DPDS, DPD and *n*Bu-PTCDA-$(CH_2)_4$-NH_2 using infrared and Raman techniques were achieved. The first two compounds were studied because of their strange behavior on gold and silver colloids, while the third one was used as target molecule in SMD measurements. In the case of sulfides, a complete assignment of fundamental vibrational frequencies was given based on observed frequencies and, for the first time, helped by *ab-initio* calculations using DFT techniques. For instance, in the past, the assignment of S-S stretching vibration in DPDS was based only on the observation of the strong band at 542 cm^{-1}. Reproducible SERS spectra were obtained on evaporated silver island films, colloidal silver and evaporated gold island films confirming the cleavage of the S-S bond in solution or in solid-state reactions with the oxidation of the metal and the formation of sulfide complex. The SERS spectra of the dissociation products showed a modest enhancement factor, which is most likely due to

the inhibition of the SERS effect by the chemical reaction with the metal nanostructures (responsible for the SERS enhancement). The strong reaction with the surface may explain the fact that the Ag-S stretching vibration is not clearly observed in the SERS spectra of published work on sulfur-metal bonds, while it was clearly observed as a shoulder in the salt complex at 244 cm^{-1} within the region of 150-250 cm^{-1}, assigned in most past publications on this topic. The observation of a S-S bond stretching in the RAIRS spectra of DPDS might explain two facts; either the molecule does not dissociate on smooth surfaces or the molecule adsorbs through only a single sulfur atom on silver and aluminum smooth mirrors. The disappearance of the C-S band in SERS spectra of DPS on silver colloid was also confirmed with two laser lines, as the C-S stretching band at 615 cm^{-1} has disappeared from the SERS spectra on various silver substrates. This band is still seen, however, in the SERS spectrum on cast gold colloids, and can be explained by the molecule's less reactivity on gold colloids. The conformation of DPS on surface might also play a role of disappearance or appearance of the band in SERS spectra. The adsorbed product formed by DPDS and DPS on the silver surfaces is actually the same.

A complete vibrational study using Raman and infrared techniques was carried out on *n*Bu-PTCDA-$(CH_2)_4$-NH_2, with targets to both; reach single molecule detection using the Raman technique and to determined the molecular orientation on evaporated silver mirror. The assignment of the vibrational fundamentals was aided by DFT calculations at B3LYP/6-31G (d) level of theory. Single molecule SERRS spectra were obtained on two different conditions, silver colloid used in liquid form and colloidal gold used in casted form. In a picomole scattering volume in colloidal silver solution, the

SERRS spectrum of about 0.01 molecule/pL was observed with the addition of 10^{-12} M of the analyte while in the case of gold casted colloids, 10^{-9} M of the analyte showed a single molecule SERRS spectrum in an area of 1 μm^2 of scattering volume. Overtones and combinations were also observed in SERRS, assigned and interpreted. The C-H wagging band at 708 cm^{-1} was weak in the RAIRS, and the flat molecular orientation on the surface is also weak. The intensity of symmetric C=O stretching vibrations at 1696 cm^{-1} in the RAIRS spectra compared to the transmission were observed. The molecule is most likely to adsorb with head-on (normal) on silver mirror. Future work can be focused on the optical properties of citrate and borohydride colloids and to study different active molecules. More investigation is needed to study the behavior of DPDS on smooth surfaces in terms of non-cleavage of S-S bond. SMS of the off resonance molecular absorption in a very dilute colloidal solution and very low analyte concentration could be the future challenge in this area of research.

The major contributions from this research work is that the understanding to some extent the surface chemistry (binding, alignment and reactivity) of two sulfide derivatives, whom behavior on the surfaces is a research subject of different groups. It illustrates the combination of Raman and metal colloid system as powerful analytical techniques to probe a single molecule at very low concentrations.

APPENDIX A: LIST OF PUBLICATIONS

- Benissa Tolaieb; Ricardo Aroca, *Canadian Journal of Analytical Science and Spectroscopy* **2003,** *2(48)*139-145.

APPENDIX B: CONFERENCE AND PRESENTATIONS

Poster Presentation:

- Benissa Tolaieb, Ricardo Aroca, "Surface-Enhanced Raman Scattering of Diphenyl Disulfide on Silver Colloids and Silver and Gold Island Films" ICASS 2002 conference, May 2002, Toronto, Canada.

REFERENCES

(1) Jeanmaire, D. L.; Van Duyne, R. P., *J. Electroanal. Chem.* **1977**, *84*, 1.

(2) Albrecht, M. G.; Creighton, J. A., *J. Am. Chem. Soc.* **1977**, *99*, 5215.

(3) Chang, R. K.; Furtak, T. E., *Surface-enhanced Raman Scattering*; Plenum Press: New York, 1982.

(4) Otto, A.; Cardona, M., Guntherodt, G., Eds., *Light Scattering in Solids IV*; Springer: Berlin, 1984.

(5) Nakatsuji, H.; Nakai, H., *Chem. Phys. Lett.* **1990**, *174*, 283.

(6) Nakatsuji, H.; Nakai, H., *J. Chem. Phys.* **1993**, *98*, 2423.

(7) Moskovits, M.; Suh, J. S., *J. Phys. Chem.* **1984**, *88*, 5526.

(8) Moskovits, M., *J. Chem. Phys.* **1982**, *77*, 4408.

(9) Sanchez-Cortes, S.; Garcia-Ramos, J. V.; Morcillo, G.; Tinti, A. *J. Colloid Interface Sci.* **1995**, *175*, 358-368.

(10) Nie, S.; Emory, S. R., *Science* **1997**, *275*, 1102.

(11) Emory, S. R.; Haskins, W. E.; Nie, S., *J. Am. Chem. Soc.* **1998**, *120*, 8009.

(12) Haslell, T. L.; Tay, L.; Moskovits, M., *J. Chem. Phys.* **2000**, *113*, 1641.

(13) Dustin, J. M.; Emory, S. R.; Nie, S., *Chem. Matt.* **2001**, *13*, 1082.

(14) Moskovits, M.; Gu, X. J.; VLckova, B., *J. Phys. Chem.* **1997**, *101*, 1588.

(15) Weitz, D. A.; Olivera, M., *Phys. Rev. Lett.* **1984**, *52*, 1433.

(16) Weitz, D. A.;Lin M, Y.; Sandroff, C. J., *Surf. Sci.* **1985**, *185*, 147.

(17) Creighton, J. A.; Alvarez, M. S.; Weitz, D. A.; Garoff, S.; Kim, M. W., *J. Phys. Chem.* **1983**, *87*, 4793.

(18) Tai, H. J.; Kwan, K.; Myung, S. K., *J. Mol. Struc.* **1987**, *162*, 191.

(19) Moskovits, M., *Rev. Modern Phys.* **1985**, *57*, 783.

(20) Shalaev, V. M., *Nonlinear optics of random media: Fractal composites and metal-dielectric films*; Springer: Berlin, Heideberg, 2000.

(21) Lee, P. C.; Meisel, D. J., *J. Phys. Chem.* **1982**, *86*, 3391.

(22) Creighton, J. A.; Blatchford, C. G.; Albrecht, M. G., *J. Chem. Soc. Faraday II* **1978**, *75*, 790.

(23) Kim, W.; Safonov, V. P.; Drachev, V. P.; Podolskiy, V. A.; Shalaev, V. M.; Armstrong, R. L., *Topics Appl. Phys.* **2002**, *82*, 149.

(24) Siiman, O.; Bumm, L. A.; Callaghan, R.; Blatchford, C. G.; Kerker, M. *J. Phys. Chem.* **1983**, *87*, 1014.

(25) Fredericks, P. M.; Sarinas, S.; Wentrup-Byrne, E., *Appl. Spectrosc.* **1993**, *47*, 1192.

(26) Yates, J. T.; Madey, T. E., *Vibrational Spectroscopy of Molecules on Surfaces*; Plenum Press: New York, 1987.

(27) Atkins, P. W., *Quanta-A Handbook of concepts*; Oxford University: Oxford, 1991.

(28) Fleishmann, M.; Van Duyne, R. P.; McQuillan, A., *Chem. Phys. Lett.* **1974**, *26*,163.

(29) Siiman, O.; Kerker, M.; Wang, D.-S., *J. Phys. Chem.* **1984**, *88*, 3168.

(30) Nakai, H.; Nakatsuji, H., *J. Chem. Phys.* **1995**, *103*, 2286.

(31) Corni, S.; Tomasi, J., *J. Chem. Phys.* **2002**, *116*, 1156.

(32) Sinther, M.; Pucci, A.; Otto, A.; Priebe, A.; Diez, S., *Phys. Stat. Sol.* **2001**, *188*, 1471.

(33) Kester, J. J.; Furtak, T. E.; Bevolo, A. J., *J. Electrochem. Soc.* **1982**, *129*, 1718.

(34) Hashemi, T.; Hogarth, C. A., *Electrochim. Acta.* **1988**, *33*, 1123.

(35) Allum, K. G.; Creighton, J. A.; Green, J. H.; Minkoff, G. J.; Prince, L. J. S., *Spectrochim. Acta,* **1968**, *24A*, 937.

(36) Sandroff, C. J.; Herschbach, D. R., *J. Phys. Chem.* **1982**, *86*, 3277.

(37) Joo; T. H.; Yim, Y. H.; Kim, K.; Kim, M. S., *J. Phys. Chem.* **1989**, *93*, 1422.

(38) Merklin, G. T.; He, L.-T.; Griffiths, P. R., *Appl. Spectrosc.* **1999**, *11*, 1448.

(39) Green, J. H. S., *Spectrochim. Acta* **1968**, *24A*, 1627.

(40) Cho, S. H.; Lee, Y. J.; Kim, M. S.; Kim, K., *Vib. Spectrosc.* **1996**, *10*, 261.

(41) Aroca, R. F.; Clavijo, R. E.; Halls, M. D.; Schlegel, H. B., *J. Phys. Chem. A* **2000**, *104*, 9500.

(42) Takahashi, M.; Fujita, M.; Ito, M., *Surf. Sci.* **1985**, *158*, 307.

(43) Joo, T. H.; Kim, M. S.; Kim, K., *J. Raman Spectrosc.* **1987**, *18*, 57.

(44) Furtak, T. E.; Reyes, J. *Surf. Sci.* **1980**, *93*, 351.

(45) Pockrand, I., *Surface enhanced Raman vibrational studies at solid/gas interfaces.*; Spriger-Verlag: Berlin, 1984.

(46) Barnes, M. D.; Whitten, W. B.; Ramsey, J. M., *Anal. Chem.* **1995**, *67*.

(47) Kneipp, K.; Wang, Y.; kneipp, H.; Itzkan, I.; Dassari, R. R.; Feld, M. S., *Phys. Rev. Lett.* **1996**, *76*, 2444.

(48) Kneipp, K.; Wang, Y.; Kneipp, H.; Perelman, L. T.; Itzkan, I.; Dasari, R. R.; Feld, M. S., *Phys. Rev. Lett.* **1997**, *78*, 1667.

(49) Nie, S.; Emory, S. R., *J. Phys. Chem. B* **1998**, *102*, 493.

(50) Kneipp, K.; Kneipp, H.; Itzkan, I.; Dasari, R. R., *Chem. Rev.* **1999**, *99*, 2957

(51) Kall, M.; Xu, H. X.; Bjerneld, E. J.; Borjesson, L., *Phys. Rev. Lett.* **1999**, *83*, 4357.

(52) Krug II, J. T.; Wang, G. D.; Emory, S. R.; Nie, S., *J. Am. Chem. Soc.* **1999**, *121*, 9208.

(53) Lecomte, S.; Moreau, N. J.; Manfait, M.; Aubard, J.; Baron, M. H., *Biospectrosc.* **1995**, *1*, 423.

(54) Aubard, J.; Bagnasco, E.; Pantigny, J.; Ruasse, M. F.; Levi, G.; Wentrup-Byrne, E., *J. Phys. Chem.* **1995**, *99*, 7078.

(55) Kneipp, K.; Kneipp, H.; Bhaskaran, K.; Ramasamy, M.; Geurt, D.; Irving, I.; Ramachandra, R. D.; Michael, S. F., *Phys. Rev. E* **1998**, *57*, R6281.

(56) Azumi, T.; McGlynn, S. P., *J. Chem. Phys.* **1965**, *42*, 1675.

(57) Kneipp, K.; Kneipp, H.; Manoharan, R.; Hanlon, E. B.; Itzkan, I.; Dasari, R. R.; Feld, M. S., *Appl. Spectrosc.* **1998**, *52*, 1493.

(58) Shorygin, P. P., *Dok. Akad. Nauk SSSR* **1952**, *87*, 201.

(59) Van Duyne, R. P.; Haller, K. I.; Altkorn, R. I., *Chem. Phys. Lett.* **1986**, *126*, 190.

(60) Brus, L.; Michaelis, A. M.; Jiang, J., *J. Phys. Chem. B* **2000**, *104*, 11965.

(61) Meixner, A. J.; Vosgrone, T.; Sackrow, M., *J. Luminesc.* **2001**, *94-95*, 147.

(62) Sallack, J.; Maiti, A. K.; Aroca, R.; Menendez, J. R., *J. Mol. Struc.* **1997**, *410-411*, 217.

(63) Lemma, T.; Aroca, R., *J. Raman Spectrosc.* **2002**, *33*, 197.

(64) Constantino, C. J. L.; Lemma, T.; Antunes, P. A.; Aroca, R., *Anal. Chem.* **2001**, *73*, 3674.

(65) Constantino, C. J. L.; Lemma, T.; Antunes, P. A.; Aroca, R. F., *Spectrochim. Acta Part A* **2002**, *58*, 403.

(66) Cohen, L. F.; Maher, R. C.; Etchegoin, P., *Chem. Phys. Lett.* **2002**, *352*, 378.

(67) Scholz, R.; Kobitski, A. Y.; Kampen, T. U.; Schreiber, M.; Zhan, D. R. T.; Jungnicle, G.; Frauenheim, T., *Phys. Stat. Sol.(b)* **2000**, *221*, 541.

(68) Persson, B. N., *J. Chem. Phys. Lett.* **1981**, *82*, 561.

(69) Weaver, G. C.; Zou, S.; Chan, H. Y. H., *Anal. Chem.* **2000**, *72*, 38A.

(70) Skadtechenco, B. O.; Aroca, R., *Spectrochim. Acta.* **2001**, *57*, 1011.

(71) Sanchez-Cortes, S.; V., Garcia-Ramos. J. V., *J. Mol. Struct.* **1992**, *274*, 33.

(72) Kim, K.; Sang, W. H.; Sang, W., *J. Appl. Spectrosc.* **2000**, *3*.

(73) Sanchez-Cortes, S.; Garcia-Ramos, J. V., *J. Raman Spectrosc.* **1992**, *23*, 61.

(74) Prochazka, M.; Srnoya, I.; Vlckova, B.; Stephanek, J.; Maly, P., *Langmiur* **1988**, *14*, 4666.

(75) Prochazka, M.; Moizes, P.; Stephanek, J.; Vlckova, B.; Turpin, P.-Y., *Anal. Chem.* **1997**, *69*, 5103.

(76) Cotton, T. M.; Kim, J. H.; Chumanov, G. D., *J. Raman Spectrosc.* **1991**, *22*, 729.

(77) Fojtik, A.; Henglein, B.; Bunsen, G., *J. Phys. Chem.* **1993**, *97*, 252.

(78) Wilenzick, R. M.; Russell, D. C.; Morris, R. M.; Marchall, S. W., *J. Chem. Phys.* **1967**, *47*, 533.

(79) Yeh, M. S.; Yang, Y. S.; Lee, H. F.; Yeh, Y. H.; Yeh, C. S., *J. Phys. Chem.B* **1999**, *103*, 6851.

(80) R. *Renishaw Inc.* **2000**.

(81) B. D. T. Manual *Bomem Inc.* **1986**.

(82) Kam, A. Ph.D. Dissertation, University of Windsor, Windsor, Windsor, Ontario, 2001.

(83) Atkins, P., *Physical Chemistry*; W. H. Freeman and company: New York, 1998.

(84) Marti, V.; Fernandez, L.; Fornes, V.; Garcia, H.; Roth, H. D., *J. Chem. Soc.* **1999**, *2*, 145.

(85) Frisch, M. J.; W.;, T. G.; Schlegel, H. B.; Scuseria, G. E.; Robb, M. A.; Cheeseman, J. R.; Zakrzewski, V. G.; Montgomery Jr, J. A.; Stratmann, R. E.; Burant, J. C.; Dapprich, S.; Millam, J. M.; Daniels, A. D.; Kudin, K. N.; Strain, M. C.; Farkas, O.; Tomasi, J.; Barone, V.; Cossi, M.; Cammi, R.; Mennucci, B.; Pomelli, C.; Adamo, C.; Clifford, S.; Ochterski, J.; Petersson, G. A.; Anyala, P. Y.; Cui, Q.; Morokuma, K.; Malick, D. K.; Rabuck, A. D.; Raghavachari, K.; Forsman, J. B.; Ciolowski, J.; V.;, O. J.; Stefanov, B. B.; Lui, G.; Liashenko, A.; Piskorz, P.; Komaromi, I.; Gomperts, R.; Martin, R. L.; Fox, D. J.; Keith, T.; Al-Laham, M. A.; Peng, C. Y.; Nanayakkara, A.; Gonzalez, C.; Challacombe, M.; Gill, P. M. W.; Johnson, B.; Chen, W.; Wong, M. W.; Andres, J. L.; Gonzalez, C.; Head-Gordon, M.; Replogle, E. S. P., J. A.; Gaussian, Inc: Pittsburgh PA., **1998**.

(86) Tolaieb, B.; Aroca, R., *Can. J. Anal. Sci. Spectrosc.* **2003,** *(48)*139.

(87) Cho, S. H.; Han, H. S.; Jang, D. J.; Kim, K.; Kim, M. S., *J. Phys. Chem.* **1995**, *99*, 10594.

(88) Bowmaker, G. A.; Tan, L. C., *Aust. J. Chem.* **1979**, *32*, 1443.

(89) Yang, X. M.; Tryk, D. A.; Ajito, K.; Hashimoto, K.; Fujishima, A., *Langmuir* **1996**, *12*, 5525.

(90) Imae, T.; Torii, H., *J. Phys. Chem. B* **2000**, *104*, 9218.

(91) Lee, H. M.; Kim, M. S.; Kim, K., *Vib. Spectrosc.* **1994**, *6*, 205.

(92) Greenler, R. G., *J. Chem. Phys.* **1969**, *50*, 1963.

(93) Greenler, R. G., *J. Chem. Phys.* **1966**, *44*, 310.

(94) Greenler, R. G., *J. Vac. Sci. Technol.* **1975**, *12*, 1410.

(95) Heavens, O. S., *Optical Properties of Thin Solid Film*: Butterworths, London, 1955.

(96) Johnson, E.; Aroca, R., *Appl. Spectrosc.* **1995**, *49*, 472.

(97) Abu-Eittah, R. H.; Hilal, R. H., *Appl. Spectrosc.* **1972**, *26*, 270.

(98) Yang, X. M.; Tryk, D. A.; Ajito, K.; Hashimoto, K.; Fujishima, A., *J. Raman Spectrosc.* **1998**, *29*, 725.

(99) Kim, K.; Kim, M. S.; Yim, Y. H., *J. Phys. Chem.* **1990**, *94*, 2552.

(100) Mercadante, R.; Trsic, M.; Duff, J.; Aroca, R., *J. Mol. Struc., Theochem* **1997**, *394*, 215.

(101) Pettinger, B.; Krischer, K., *J. Electron Spectrosc. Relat. Phenom.* **1987**, *45*, 133.

(102) Clavijo, R. E., Aroca, R., *Spectrochim. Acta, Part A* **1991**, *47*, 271.

(103) Rodriguez-LIorente, S.; Aroca, R.; Duff, J., *J. Mater. Chem.* **1998**, *3*, 629.

(104) Goulet, P. J. G.; Pieczonka, N. P. W., Aroca, R. F., *published on line March, J. Anal. Chem.* **2003**.

(105) Okamoto, H.; Sekimoto, Y.; Tasumi, M., *Spectrochim. Acta* **1994**, *50A*, 1467.

VITA AUCTORIS

BIRTHDATE:	September 8th, 1967	Hig Hgail, Mourzouk, Libya
EDUCATION:	1986-1990	University of Sebha, Libya.
	Since 1993	Waha Oil Company, Libya.
	2000-2003	University of Windsor
		Windsor, Ontario, Canada.